

High-dimensional Bayesian model selection by proximal nested sampling

Xiaohao Cai*, Jason D. McEwen†, and Marcelo Pereyra‡

Abstract. Imaging methods often rely on Bayesian statistical inference strategies to solve difficult imaging problems. Applying Bayesian methodology to imaging requires the specification of a likelihood function and a prior distribution, which define the Bayesian statistical model from which the posterior distribution of the image is derived. Specifying a suitable model for a specific application can be very challenging, particularly when there is no reliable ground truth data available. Bayesian model selection provides a framework for selecting the most appropriate model directly from the observed data, without reference to ground truth data. However, Bayesian model selection requires the computation of the marginal likelihood (Bayesian evidence), which is computationally challenging, prohibiting its use in high-dimensional imaging problems. In this work we present the *proximal nested sampling* methodology to objectively compare alternative Bayesian imaging models, without reference to ground truth data. The methodology is based on nested sampling, a Monte Carlo approach specialised for model comparison, and exploits proximal Markov chain Monte Carlo techniques to scale efficiently to large problems and to tackle models that are log-concave and not necessarily smooth (e.g., involving ℓ_1 or total-variation priors). The proposed approach can be applied computationally to problems of dimension $\mathcal{O}(10^6)$ and beyond, making it suitable for high-dimensional inverse imaging problems. It is validated on large Gaussian models, for which the likelihood is available analytically, and subsequently illustrated on a range of imaging problems where it is used to analyse different choices for the sparsifying dictionary and measurement model.

Key words. Nested sampling, MCMC sampling, marginal likelihood, Bayesian evidence, inverse problems, proximal optimisation, model selection

1. Introduction. High-dimensional inverse problems are ubiquitous in the imaging sciences, as well as in the physical and engineering sciences more generally. Due to limitations of the data observation process and measurement noise, or even just due to the nature of the problem at hand, most inverse problems encountered in imaging are seriously ill-conditioned or ill-posed (canonical examples include, e.g., medical and radio interferometric imaging [12, 6, 47, 23]). Developing better methodology for solving challenging imaging inverse problems is a significant focus of the community. Several frameworks have been proposed in the literature to derive accurate solutions that are well-posed, accurate, and computationally efficient [21] (a problem is well-posed in the sense of Hadamard if a solution exists, is unique, and stable to perturbations of the observed data).

The Bayesian statistical framework is currently one of the predominant frameworks to perform inference in inverse imaging problems [39, 36]. Bayesian methods start by specifying a joint statistical model for the observed data and the unknown image of interest, defined by a likelihood function and a prior distribution, respectively. From the joint statistical model

*Mullard Space Science Laboratory (MSSL), University College London (UCL), Surrey RH5 6NT, UK. School of Electronics and Computer Science, University of Southampton, Southampton SO17 1BJ, UK (x.cai@soton.ac.uk).

†Mullard Space Science Laboratory (MSSL), University College London (UCL), Surrey RH5 6NT, UK (jason.mcewen@ucl.ac.uk).

‡School of Mathematical and Computer Sciences, Heriot-Watt University, Edinburgh, Scotland, UK (m.pereyra@hw.ac.uk).

stems the posterior distribution of the unknown image given the observed data, which is the basis for image estimators and for quantifying uncertainties [38, 12, 47, 34]. Special attention is given in the literature to posterior distributions that are log-concave, i.e., associated with a convex potential function, as this enables the use of highly efficient Bayesian computation methods based on scalable proximal optimisation algorithms [7] and proximal Markov chain Monte Carlo (MCMC) algorithms [12, 45].

Of course, the choice of the Bayesian model used has a profound impact on the solutions delivered, as alternative models can lead to significantly different point estimations and uncertainty quantification results. As a consequence, applied Bayesian imaging scientists devote an important part of their efforts to developing application specific models that are accurate, robust, and amenable to efficient computation, e.g., [40, 3, 47, 5, 23]. This is mainly related to the choice of suitable parametric forms for the likelihood and prior defining the model. Model parameters (e.g., regularisation weights, noise variance, etc.) can often be adjusted automatically by using modern Bayesian model calibration techniques (see, e.g., [46]).

There is an important related question that remains largely unexplored in the imaging literature: namely, how to objectively compare alternative Bayesian imaging models to decide which model is most appropriate for image restoration and other inference tasks. The imaging community has traditionally addressed model selection through benchmark experiments involving ground truth data. However, for many imaging problems it is difficult and expensive to produce reliable ground truth data. Moreover, for many scientific imaging problems it is simply impossible. Bayesian model selection provides a framework for selecting the most appropriate model directly from the observed data, without reference to ground truth data.

Bayesian model selection requires the computation of the *marginal likelihood* of the data – the average likelihood of a model over its prior probability space – which is also called the *Bayesian evidence*. This quantity is a key ingredient of model selection statistics such as Bayes factors and likelihood ratio tests [38]. The computation of the marginal likelihood for imaging models is highly non-trivial because it requires the computation of a high-dimensional integral, with dimension given by the number of parameters (e.g. pixels) of interest, which for imaging problems frequently reach sizes of $\mathcal{O}(10^5)$ to $\mathcal{O}(10^6)$ and beyond. For such high-dimensional settings evaluation of the marginal likelihood has been previously considered to be computationally intractable. Broadly speaking, general purpose Monte Carlo methods can only handle model selection tasks for problems of dimension $\mathcal{O}(10)$ to $\mathcal{O}(10^2)$ (for reviews see [10, 16]). Nested sampling [42], a state-of-the-art Monte Carlo strategy designed specifically for model selection, has enabled model selection for moderate dimensional problems of size $\mathcal{O}(10^2)$ to $\mathcal{O}(10^3)$ [25, 13, 14, 1, 15, 19]. To the best of our knowledge, model selection for larger problems is currently possible only for models with very specific structures (e.g., conditionally Gaussian models [20]). We address the difficult computation of the marginal likelihood by proposing a new methodology that carefully integrates nested sampling [42] with proximal MCMC sampling [33, 12].

In this work we present the *proximal nested sampling* methodology to objectively compare alternative Bayesian imaging models, without reference to ground truth data. The proposed approach is suitable for the common class of imaging models that are log-concave and potentially not smooth. Furthermore, it can be applied computationally to problems of dimension $\mathcal{O}(10^6)$ and beyond, making it suitable for high-dimensional inverse imaging problems. We

demonstrate the approach with a range of imaging models.

The remainder of the article is organised as follows. In Section 2 we introduce the Bayesian inference framework with a focus on Bayesian computation for inverse imaging problems and on Bayesian model selection. In Section 3 we recall the standard nested sampling method. Our proposed proximal nested sampling framework is presented in general form in Section 4. In Section 5 explicit forms of proximal nested sampling are presented for common forms of the likelihood and prior that arise in imaging sciences. Experimental results validating the proposed method and showcasing its use are reported in Section 6. Finally, we conclude in Section 7.

2. Bayesian inference for imaging problems. In this article we consider methodology for objectively comparing several alternative Bayesian models when solving an imaging problem. The aim is automatic model selection in imaging problems when no ground truth is available. We focus on Bayesian models with posterior distributions that are log-concave, for which maximum-a-posteriori estimation is a convex optimisation problem. From a computational perspective, these are models where Bayesian inference is efficiently performed by using state-of-the-art proximal optimisation and proximal MCMC methods, which were specifically designed for large-scale problems with an underlying convex geometry, as often encountered in the imaging sciences.

In this section we define some elements of convex analysis which are essential for our method, recall the Bayesian decision-theoretic approach to model comparison, and briefly review proximal MCMC methods, which are an important component of the proximal nested sampling methodology proposed in Section 4. We conclude the section by briefly explaining the computational difficulties encountered in Bayesian model selection and why it is necessary to develop new methodology for this task.

2.1. Convex analysis. Let $f : \mathbb{R}^d \rightarrow (-\infty, +\infty)$. The function f is said to be proper if there exists $x_0 \in \mathbb{R}^d$ such that $f(x_0) < +\infty$. Denote for all $M \in \mathbb{R}$, $\{f \leq M\} = \{z \in \mathbb{R}^d \mid f(z) \leq M\}$. The function f is lower semicontinuous (l.s.c.) if for all $M \in \mathbb{R}$, $\{f \leq M\}$ is a closed subset of \mathbb{R}^d . For $k \geq 0$, denoted by $\mathcal{C}^k(\mathbb{R}^d)$ the set of k -times continuously differentiable functions. For $f \in \mathcal{C}^1(\mathbb{R}^d)$, denote by ∇f the gradient of f . We say that $f \in \mathcal{C}^1(\mathbb{R}^d)$ is a Lipschitz continuously differentiable function if there exists $C \geq 0$ such that for all $x, y \in \mathbb{R}^d$, $\|\nabla f(x) - \nabla f(y)\| \leq C\|x - y\|$.

Given a convex, proper, l.s.c. function $h : \mathbb{R}^d \rightarrow (-\infty, +\infty]$ and $\lambda > 0$, the proximal operator [32] associated with function h at $x \in \mathbb{R}^d$ is defined as

$$(2.1) \quad \text{prox}_h^\lambda(x) = \underset{u \in \mathbb{R}^d}{\operatorname{argmin}} \{h(u) + \|u - x\|_2^2/2\lambda\}.$$

When $\lambda = 1$, we denote $\text{prox}_h^1(x)$ by $\text{prox}_h(x)$ for simplicity.

Let \mathcal{K} be a closed convex set in \mathbb{R}^d and let $\chi_{\mathcal{K}}$ be the characteristic function for \mathcal{K} , defined by $\chi_{\mathcal{K}}(x) = 0$ if $x \in \mathcal{K}$ and $+\infty$ otherwise. The proximal operator of $\chi_{\mathcal{K}}$ is the projection onto \mathcal{K} , given by

$$(2.2) \quad \text{proj}_{\mathcal{K}}(x) = \underset{u \in \mathbb{R}^d}{\operatorname{argmin}} \{\chi_{\mathcal{K}}(u) + \|u - x\|_2^2/2\}.$$

The convex conjugate of function h , denoted by h^* , is defined as

$$(2.3) \quad h^*(x) = \sup_{u \in \mathbb{R}^d} \{x^\top u - h(u)\}.$$

Its proximal operator can be related to the proximal operator of h by

$$(2.4) \quad \text{prox}_{h^*}(x) = x - \text{prox}_h(x).$$

The λ -Moreau-Yosida envelope of h [32] is given for any $x \in \mathbb{R}^d$ and $\lambda > 0$ by

$$(2.5) \quad h^\lambda(x) = \min_{u \in \mathbb{R}^d} \{h(u) + \|u - x\|_2^2/2\lambda\}.$$

The envelope h^λ is continuously differentiable with Lipschitz gradient. In particular, using the proximal operator, the gradient of h^λ can be written

$$(2.6) \quad \nabla h^\lambda(x) = (x - \text{prox}_h^\lambda(x))/\lambda,$$

with λ simultaneously controlling the Lipschitz constant of ∇h^λ as well as the error between h and its smooth approximation h^λ . This approximation error can be made arbitrarily small by reducing λ , at the expense of deteriorating the regularity of ∇h^λ .

2.2. Bayesian estimation and model selection. Let $\Omega \subseteq \mathbb{R}^d$. We consider the estimation of an unknown image $x \in \Omega$ from observed data y . Bayesian methods address such problems by postulating a statistical model \mathcal{M} relating x and y , from which estimators of x and other inferences can be derived. More precisely, \mathcal{M} defines a joint probability distribution $p(x, y | \mathcal{M})$ specified via the decomposition $p(x, y | \mathcal{M}) = p(y | x, \mathcal{M})p(x | \mathcal{M})$, where $p(y | x, \mathcal{M})$ denotes the likelihood of x for the observed data y , and the marginal $p(x | \mathcal{M})$ is the so-called prior of x . Following Bayes' theorem, inferences on $x | y$ are then based on the posterior distribution

$$(2.7) \quad p(x | y, \mathcal{M}) = \frac{p(y | x, \mathcal{M})p(x | \mathcal{M})}{p(y | \mathcal{M})},$$

which models our beliefs about x after observing y . As it is often the case in imaging sciences, we focus on posterior distributions that are log-concave and assume that the potential function $x \mapsto -\log p(x | y, \mathcal{M})$ is convex l.s.c. on Ω , but possibly not smooth.

We condition on \mathcal{M} explicitly in (2.7) because our focus is model selection, where one entertains several alternative posterior distributions for $x | y$ stemming from different underlying modelling assumptions. As a result, rather than the posterior $p(x | y, \mathcal{M})$, our main object of interest is the *marginal likelihood* or *model evidence*

$$(2.8) \quad p(y | \mathcal{M}) = \int_{\Omega} p(y, x | \mathcal{M}) dx = \int_{\Omega} p(y | x, \mathcal{M})p(x | \mathcal{M}) dx,$$

which measures the likelihood of the observed data under model \mathcal{M} , and which we use to objectively compare different models relating x and y [38]. Notice that the likelihood of the observed data y under the model \mathcal{M} is essentially the expectation (or average value) of the likelihood function $p(y | x, \mathcal{M})$ with respect to (w.r.t.) the prior $p(x | \mathcal{M})$. Therefore, a model

that allocates its prior mass to solutions that agree with the observed data achieves a large marginal likelihood value. Conversely, a low marginal likelihood value indicates that only a small proportion of the solutions favoured by the prior agree with the observed data. In other words, the marginal likelihood (2.8) measures the degree to which the observed data is in agreement with the assumptions of the model, and in doing so it provides a goodness-of-fit summary. Moreover, because all priors have the same total probability mass (i.e., $\int_{\Omega} p(x)dx = 1$), the likelihood (2.8) naturally incorporates Occams's razor, trading off model simplicity and accuracy and penalising over-fitting [38].

Bayesian model selection arises from the common and natural inquiry of which model is the most suitable to analyse $x|y$ from a set of alternative models $\mathcal{M}_1, \dots, \mathcal{M}_K$ available. For simplicity and without loss of generality, we suppose two alternative models \mathcal{M}_1 and \mathcal{M}_2 (the generalisation to additional models is straightforward). From Bayesian decision theory, to objectively compare the two models in settings without ground truth available, one should calculate the *Bayes factor* [38]

$$(2.9) \quad \rho_{12} = \frac{p(\mathcal{M}_1|y) p(\mathcal{M}_2)}{p(\mathcal{M}_2|y) p(\mathcal{M}_1)}$$

where $p(\mathcal{M}_1)$ and $p(\mathcal{M}_2)$ denote the prior probabilities assigned to the two competing models, and where, from Bayes' theorem, we have that for any $i \in \{1, 2\}$

$$p(\mathcal{M}_i|y) = \frac{p(y|\mathcal{M}_i)p(\mathcal{M}_i)}{p(y|\mathcal{M}_1)p(\mathcal{M}_1) + p(y|\mathcal{M}_2)p(\mathcal{M}_2)}.$$

By developing (2.9) we can easily express the Bayes factor as the likelihood ratio

$$(2.10) \quad \rho_{12} = \frac{p(y|\mathcal{M}_1)}{p(y|\mathcal{M}_2)},$$

highlighting that ρ_{12} is invariant to choice of the prior probabilities $p(\mathcal{M}_1)$ and $p(\mathcal{M}_2)$. If one assumes $p(\mathcal{M}_1) = p(\mathcal{M}_2) = 1/2$ to reflect the absence of prior information, then the factor also coincides with the posterior probability ratio $p(\mathcal{M}_1|y)/p(\mathcal{M}_2|y)$.

Being a likelihood ratio, the factor ρ_{12} is straightforward to read: if $\rho_{12} \gg 1$, we prefer model \mathcal{M}_1 over the alternative \mathcal{M}_2 ; conversely, if $\rho_{12} \ll 1$, we prefer model \mathcal{M}_2 ; and if $\rho_{12} \approx 1$, we do not prefer either, inasmuch as the data y are insufficient for us to make an informed judgement.

Unfortunately, calculating ρ_{12} is generally not possible in imaging sciences because the dimensionality of x renders the marginal likelihoods $p(y|\mathcal{M}_1)$ and $p(y|\mathcal{M}_2)$ computationally intractable. More precisely, the marginal likelihoods are doubly-intractable because they require computing two intractable integrals over the space of solutions Ω : the marginalisation of x denoted explicitly in (2.8); and the normalising constant of the priors $p(x|\mathcal{M}_i)$ when these are not available analytically, which otherwise implicitly also requires integrating over Ω .

It is worth emphasising at this point that this major difficulty related to model selection is not encountered when performing inferences with the posteriors $p(x|y, \mathcal{M}_1)$ and $p(x|y, \mathcal{M}_2)$ individually. The reason is that MCMC methods have been designed precisely to enable sampling from $p(x|y, \mathcal{M})$ without ever having to evaluate the marginal likelihood $p(y|\mathcal{M})$. As a

result, efficient model selection remains an open problem in imaging sciences, whereas posterior inferences such as point estimation and uncertainty quantification can be now computed with relative ease by using specialised MCMC approaches. The development of efficient Bayesian computation methodology for model selection in imaging problems is precisely the focus of the current article.

In the following we briefly recall MCMC sampling, particularly proximal MCMC techniques specialised for imaging problems, and explain why they are not suitable for comparing imaging models in a computationally efficient manner.

2.3. Bayesian computation and proximal MCMC methods. Consider the problem of calculating probabilities or expectations w.r.t. to some distribution $\pi(dx)$ which admits a density $\pi(x)$ w.r.t the usual d -dimensional Lebesgue measure. In the context of Bayesian inference, this is typically the posterior $p(x|y, \mathcal{M})$. Evaluating expectations and probabilities w.r.t. π is non-trivial in problems of moderate and high dimension because of the integrals involved, which are usually beyond the scope of analytical and deterministic numerical integration schemes. These calculations are further complicated when the normalising constant of π is not known, as this requires evaluating an additional d -dimensional integral.

Engineering and physical sciences usually address the computation of probabilities and expectations w.r.t. π by simulating a set of samples from π followed by Monte Carlo stochastic integration. While there are different ways of simulating samples from π , most methods adopt an MCMC strategy where one proceeds by constructing a Markov chain that has π as its invariant stationary distribution. Again, there are different methods for constructing such Markov chains, but most applications in inverse problems use the Metropolis-Hastings (MH) method [39], Gibbs sampling [39], Hamiltonian Monte Carlo [28], and slice sampling [27]. We refer the interested reader to [39] for an excellent introduction to MCMC methodology, and to [18] for a survey of recent developments in the Bayesian computation literature.

The fastest MCMC methods for imaging problems of the form (2.7) are derived from the overdamped Langevin diffusion process, which we recall below. For simplicity, rather than presenting the Langevin approach in full generality, we focus our presentation on proximal Langevin sampling for non-smooth models, which we later use in the proximal nested sampling method proposed in Section 4. For a more exhaustive introduction to the topic please see [45, Section 2] and references therein.

Assume that π admits a decomposition $\pi(x) \propto \exp\{-f(x) - g(x)\}$ for all $x \in \mathbb{R}^d$, where $f \in \mathcal{C}^1(\mathbb{R}^d)$ with ∇f Lipschitz continuous with constant L_f , and where g is a proper l.s.c. function that is convex on \mathbb{R}^d but potentially non-smooth (e.g., g could encode constraints on the solution space and involve non-smooth regularisers such as the ℓ_1 norm). To simulate from π , we construct the overdamped Langevin stochastic differential equation (SDE) on \mathbb{R}^d given by [12]

$$(2.11) \quad dX_t = -\nabla f(X_t) - \nabla g^\lambda(X_t)dt + \sqrt{2}dW_t, \quad X_0 = x_0,$$

where $(W_t)_{t \geq 0}$ is a d -dimensional Brownian motion, g^λ is the Moreau-Yosida envelop of g given by (2.5), $\lambda > 0$ is a smoothing parameter that we will discuss later, and $x_0 \in \mathbb{R}^d$. When $x \rightarrow f(x) + g^\lambda(x)$ is convex, the SDE has a unique strong solution and X_t converges exponentially fast (as $t \rightarrow \infty$) to an invariant measure that is in the neighbourhood of π .

To use (2.11) for Bayesian computation, we use a numerical solver to compute a discrete-time approximation of X_t over some time period $t \in [0, T]$; the resulting discrete sample path constitutes our set of Monte Carlo samples. In particular, in this paper we use the conventional Euler-Maruyama approximation

$$(2.12) \quad X_{n+1} = X_n - \frac{\delta}{2} \nabla f(X_n) - \frac{\delta}{2} \nabla g^\lambda(X_n) + \sqrt{\delta} Z_{n+1},$$

where $\delta \in [0, 1/(L_f + 1/\lambda)]$ is a given stepsize and $(Z_n)_{n \geq 1}$ is a sequence of i.i.d. d -dimensional standard Gaussian random variables. This MCMC method is known as the Moreau-Yosida unadjusted Langevin algorithm (MYULA) [12]. The Markov chain (2.12) is usually implemented by using (2.6) and reads

$$(2.13) \quad X_{n+1} = X_n - \frac{\delta}{2} \nabla f(X_n) - \frac{\delta}{2\lambda} \left(X_n - \text{prox}_g^\lambda(X_n) \right) + \sqrt{\delta} Z_{n+1}.$$

The smoothing parameter λ and the stepsize δ jointly control a bias-variance trade-off between the asymptotic estimation errors and non-asymptotic errors associated with using a finite number of iterations. Large values of λ and δ lead to faster convergence to stationarity but also more asymptotic bias. In this paper, we use $\lambda = 1/L_f$ and $\delta = 0.8/(L_f + 1/\lambda)$ as recommended in [12]. Please see [12, 45] for more details.

The samples generated by (2.13) can be directly used for biased Monte Carlo estimation [12]. Alternatively, at the expense of additional computation, one can supplement each iteration of MYULA with an MH (Metropolis-Hastings) correction step to asymptotically remove the approximation errors related to the discretisation of the SDE and to use g^λ instead of g , leading to a type of Metropolis-adjusted Langevin algorithm (MALA) (see [33] for details).

2.4. Monte Carlo estimation of marginal likelihoods and Bayes factors. Let $\{X_n\}_{n=1}^N$ be a set of samples from π (or an approximation of π), generated by using a proximal MCMC method or otherwise. Following a Monte Carlo (stochastic) numerical integration approach, the expectation of any function $\phi : \mathbb{R}^d \rightarrow \mathbb{R}$ w.r.t. π is approximated by taking the sample average

$$(2.14) \quad \hat{E}_\pi(\phi) = \frac{1}{N} \sum_{n=1}^N \phi(X_n),$$

which, under assumptions, converges to the truth $E_\pi(\phi) = \int_\Omega \phi(x) \pi(x) dx$ as N increases (or to a biased estimate if the samples are not exactly from π). The accuracy of Monte Carlo estimates depends of course on the number of samples N and on the properties of the MCMC method used, but it also depends crucially on the variance $\text{Var}_\pi(\phi)$. Unfortunately, $\text{Var}_\pi(\phi)$ is often very large for the kinds of functions ϕ required for estimating the marginal likelihood (2.8) (and in some cases $\text{Var}_\pi(\phi)$ is not even defined), leading to Monte Carlo estimators of the marginal that behave poorly [30]. As a result, it is difficult to use the samples $\{X_n\}_{n=1}^N$ to perform model selection.

Several strategies have been proposed in the computational statistics literature to address the aforementioned difficulty and derive well-posed estimators for the marginal likelihood

(2.8) and the Bayes factor (2.9). One natural strategy is to construct a truncated estimator by first using the samples $\{X_n\}_{n=1}^N$ to identify a suitable truncating set \mathcal{A} , followed by a sample average (2.14) only with the samples verifying $X_n \in \mathcal{A}$ [2]. Although by construction well-posed, truncated estimators need to be de-biased by using the volume of \mathcal{A} , which is usually very expensive to compute when the dimension d is large. From the results of Brosse et al. [2], we believe that this strategy is unlikely to produce scalable methods suitable for imaging problems. One can circumvent or simplify the calculation of the volume of \mathcal{A} , e.g., see [12], but in our experience the resulting estimators become unstable and are difficult to use. Another avenue for stable Monte Carlo estimators for (2.8) and (2.9) is to generate samples from a sequence of distributions bridging π to some tractable reference π_0 such as the prior distribution or a Gaussian approximation of π (see, e.g., thermodynamic integration [31] and annealed importance sampling [26]). Again, the results of [2] suggest that such computation strategies are unlikely to scale efficiently to imaging problems because the number of intermediate distributions grows quickly as d increases. Many other alternatives are described in the literature, such as the Savage–Dickey density ratio [44] and Reversible Jump MCMC [17], which are mainly useful for nested or small models (for reviews of classical methods see, e.g., [16, 10]). Another alternative approach, which is agnostic to the sampling method, is the harmonic mean estimator [30]; although, in its original form the variance of the estimator can be very poorly behaved such that the estimator can be highly inaccurate in practice. Strategies to resolve this issue have been developed in the recently proposed learnt harmonic mean estimator [24], which has been shown to be highly effective and can scale to dimension $\mathcal{O}(10^3)$ and beyond. Nevertheless, it would likely be difficult to scale this approach to the high-dimensional setting required for imaging problems. One can also consider the widely used Laplace’s method [43], which relies on the assumption that the posterior distribution can be adequately approximated by a Gaussian distribution. Unfortunately, this is a strong assumption that often leads to inaccurate estimates in imaging applications. It is worth mentioning that there are also some model selection strategies that do not rely on the computation of the marginal likelihood, see e.g., [22, 35], however these are usually very computationally intensive.

A promising approach to derive computationally efficient estimators for (2.8) and (2.9) is to construct Rao-Blackwellized estimators by carefully introducing auxiliary variables, as proposed in the seminal papers by Chibb et al. [8, 9]. This strategy has been recently successfully applied to signal and image processing models that are conditionally Gaussian given conjugate model hyper-parameters [20]. Some generalisations are possible, but constructing efficient Rao-Blackwellized estimators for more general classes of models, e.g., log-concave models of the form (2.7), is highly non-trivial.

Lastly, nested sampling provides a distinctively different approach for efficiently estimating (2.8) and (2.9) [42]. The key idea in [42] underpinning nested sampling is the re-parameterisation of the marginal likelihood (2.8) as a one-dimensional integral of the likelihood with respect to the enclosed prior volume. This greatly reduces the computation costs involved, provided that one can efficiently sample from the prior distribution subject to a hard constraint on the likelihood value. Nested sampling therefore shifts the computational challenge from the direct evaluation of a high-dimensional integral to sampling of the prior subject to a hard likelihood constraint. The generation of samples is challenging and previous

works have considered a range of sampling strategies. For example, conventional MCMC sampling [42], rejection sampling (e.g. [25, 13, 14]), slice sampling (e.g. [19]), and more advanced MCMC samplers such as Galilean Monte Carlo [15] and diffusive nested sampling [1]. Following over a decade of active research, nested sampling is now a well-established technique for computing the marginal likelihood that has found widespread application, particularly in astronomy [13, 14, 44]. Nevertheless, broadly speaking, current nested sampling techniques remain restricted to moderate dimensional problems of size $\mathcal{O}(10^2)$ to $\mathcal{O}(10^3)$.

With imaging problems in mind, this article presents an efficient nested sampling methodology specifically designed for high-dimensional log-concave models of the form (2.7). A significant novelty of the proposed approach is that we address the difficult generation of samples by using a proximal MCMC technique that is naturally suited for dealing with high-dimensional log-concave distributions subject to hard convex constraints. Moreover, the proximal nature of the method straightforwardly allows the use of the non-smooth priors that are frequently encountered in imaging (e.g., involving the ℓ_1 and total-variation regularisers), which would not be easily addressed by using alternative gradient-based samplers. Section 3 below reviews the nested sampling approach. The proposed proximal nested sampling methodology is presented in Section 4.

3. Nested sampling. For ease of notation, given a model \mathcal{M} , let $\mathcal{L}(x) = p(y|x, \mathcal{M})$ denote the likelihood function, $\pi(x) = p(x|\mathcal{M})$ the prior, and

$$(3.1) \quad \mathcal{Z} = p(y|\mathcal{M}) = \int_{\Omega} \mathcal{L}(x)\pi(x)dx,$$

the marginal likelihood or evidence associated with a given model \mathcal{M} .

Nested sampling [42] was proposed specifically to facilitate the efficient evaluation of \mathcal{Z} for Bayesian model selection, while also supporting posterior inferences. As mentioned previously, the calculation of the multidimensional marginal likelihood integral (3.1) is generally computationally intractable. Nested sampling addresses this difficulty by cleverly converting (3.1) to a one-dimensional integral by re-parameterising the likelihood in terms of the enclosed prior volume. In addition, nested sampling involves the prior via simulation and hence does not require knowledge of the prior normalising constant. As a result, it also circumvents the second level of intractability of \mathcal{Z} that arises in imaging problems.

Let $\Omega_{L^*} = \{x|\mathcal{L}(x) > L^*\}$, which groups the parameter space Ω into a series of nested subspaces according to the level-set or iso-likelihood contour $\mathcal{L}(x) = L^* \geq 0$. Note that $\Omega_{L^*=0} = \Omega$, since the likelihood values cannot be negative. Define the prior volume ξ by $d\xi = \pi(x)dx$, where

$$(3.2) \quad \xi(L^*) = \int_{\Omega_{L^*}} \pi(x)dx.$$

Note that $\xi(0) = 1$ and $\xi(L_{\max}) = 0$, where L_{\max} is the maximum of the likelihood in Ω . Let $\mathcal{L}(\xi)$ be the inverse of the prior volume $\xi(L^*)$ such that $\mathcal{L}(\xi(L^*)) = L^*$, and assume it is a monotonically decreasing function of ξ (which is satisfied up to practical numerical considerations that can be trivially overcome [41]). The marginal likelihood integral (3.1) can

then be rewritten as

$$(3.3) \quad \mathcal{Z} = \int_0^1 \mathcal{L}(\xi) d\xi,$$

which is a one-dimensional integral over the prior volume ξ .

To evaluate (3.3) in practice it is necessary to compute likelihood level-sets (iso-contours) L_i , which correspond to prior volumes $0 < \xi_i \leq 1$ satisfying (3.2). A strategy to generate the likelihoods L_i and associated prior volumes ξ_i is discussed in Section 3.2. Once the likelihoods $L_i = \mathcal{L}(\xi_i)$ are obtained, (3.3) can be used to evaluate the marginal likelihood, where $\{\xi_i\}_{i=0}^N$ is a sequence of decreasing prior volumes, i.e.,

$$(3.4) \quad 0 < \xi_N < \dots < \xi_1 < \xi_0 = 1.$$

After discretising the integral (3.3) and associating each likelihood L_i a quadrature weight w_i , the marginal likelihood can be computed numerically using standard quadrature methods to give

$$(3.5) \quad \mathcal{Z} \approx \sum_{i=1}^N L_i w_i.$$

The simplest assignment of the quadrature weights is $w_i = \xi_{i-1} - \xi_i$. Alternatively, the trapezium rule can be used, i.e., $w_i = (\xi_{i-1} - \xi_{i+1})/2$. The approximation error related to the discretisation of (3.3) can be made arbitrarily small by increasing N .

3.1. Posterior inferences. Posterior inferences can be easily computed once \mathcal{Z} is found. Any sample taken randomly in the prior volume interval (ξ_{i-1}, ξ_i) is simply assigned an importance weight

$$(3.6) \quad p_i = \frac{L_i w_i}{\mathcal{Z}}.$$

Samples with the assigned weights $\{p_i\}$ can then be used to calculate posterior inferences such as the posterior moments, probabilities, and credible regions.

3.2. Marginal likelihood evaluation. We now recall the basic procedure of the standard nested sampling framework for evaluating the marginal likelihood, i.e. to compute the summation (3.5). In particular, it is necessary to generate samples of the likelihoods L_i and to estimate the corresponding enclosed prior volume ξ_i .

Firstly, set the iteration number $i = 0$, the prior volume $\xi_0 = 1$, and draw N_{live} *live* samples of the unknown image x from the prior distribution $\pi(x)$. Secondly, remove the sample with the smallest likelihood, say L_{i+1} , from the live set and replace it with a new sample. This new sample is again drawn from the prior, but constrained to a higher likelihood than L_{i+1} .

It is necessary to then determine the prior volume ξ_{i+1} enclosed by the likelihood level-set (iso-contour) defined by L_{i+1} . This is estimated in a stochastic manner. The enclosed prior volume for each step i can be estimated by a shrinkage ratio (random variable) t_{i+1} , i.e. by

$\xi_{i+1} = t_{i+1}\xi_i$, where t_{i+1} follows the distribution¹

$$(3.7) \quad p(t) = N_{\text{live}} t^{N_{\text{live}}-1}.$$

Repeat the above step (removing the sample with the smallest likelihood and estimating the updated prior volume) until the entire prior volume (and the nested shells of likelihood) has been traversed. We finally obtain $\{L_i\}$ and $\{\xi_i\}$ which can then be used to compute the marginal likelihood by (3.5). Moreover, we also simultaneously obtain a set of samples of the parameter x comprising all the discarded (dead) samples and the N_{live} final live samples, which can be used for posterior parameter inferences (refer to Section 3.1 for more detail).

The volume prior at step i of the nested sampling algorithm, is $\xi_i = \prod_{k=1}^i t_k$; recall that t_k is the shrinkage ratio and is independently distributed following the probability density function given in (3.7). Since the mean and standard deviation of $\log t$ are respectively

$$(3.8) \quad E(\log t) = -1/N_{\text{live}} \quad \text{and} \quad \sigma(\log t) = 1/N_{\text{live}},$$

we have

$$(3.9) \quad \log \xi_i \approx -i/N_{\text{live}} \pm \sqrt{i}/N_{\text{live}}.$$

Ignoring uncertainty, one thus takes

$$(3.10) \quad \xi_i = \exp(-i/N_{\text{live}}).$$

A convergence criteria for the nested sampling algorithm should be adopted. Terminating the algorithm too early or late should be avoided to ensure the marginal likelihood is estimated accurate without unnecessary additional computational cost. One stopping criterion is that the difference in marginal likelihood estimates between two iterations falls below a predefined threshold, while another is to ensure a sufficient number of dead samples is used.

The pseudo code for the nested sampling algorithm is given in Algorithm 3.1. Observe that the most challenging task in the nested sampling algorithm is drawing samples from the prior with the hard constraint that samples lie within Ω_{L_i} , i.e. within the space defined by the likelihood level-set (see item 7 in Algorithm 3.1). This constrained sampling step is relatively easy in small problems but can become very computationally challenging as problem dimension increases. As a result, nested sampling is usually restricted to problems of moderate size.

3.3. Error estimation. If the prior volumes $\{\xi_i\}$ considered in the discretised integral (3.5) used to evaluate the marginal likelihood could be assigned exactly, then the only error in the estimate of the marginal likelihood would be due to the discretisation of the integral, which is trivially $\mathcal{O}(1/N^2)$ and negligible when N is sufficiently large. However, since the shrinkage ratio t_i is generated randomly, each prior volume ξ_i is then assigned approximately, which tends to overwhelm the error brought by the discretisation of the integral and will therefore

¹The probability distribution (3.7) is for the largest of N_{live} samples drawn uniformly from the interval $[0, 1]$). This follows since the parameter x is uniformly sampled from the prior $\pi(x)$ and $\{\xi_i\}$ are uniformly distributed (by the relation $d\xi = \pi(x)dx$).

Algorithm 3.1 Nested sampling algorithm

Initialization: Data Y . Set $\mathcal{Z} = 0$, $\xi_0 = 1$ and $i = 0$. Draw N_{live} samples $\{x_n\}_{n=1}^{N_{\text{live}}}$ from the prior distribution $\pi(x)$ in the prior space Ω .

Output: Evidence \mathcal{Z} and posterior probabilities $\{p_i\}$.

for $i = 1, \dots$, until the stopping criterion reached

- Find the lowest likelihood, say L_i , in the set of live samples.
- Compute weight $w_i = (\xi_{i-1} - \xi_{i+1})/2$, where $\xi_i = \exp(-i/N_{\text{live}})$.
- Update evidence by $\mathcal{Z} = \mathcal{Z} + L_i w_i$.
- Draw a new sample from the prior distribution $\pi(x)$ in the restricted parameter space Ω_{L_i} , and replace the individual sample associated with the lowest likelihood L_i in the set of live samples.

end for

Update the evidence by $\mathcal{Z} = \mathcal{Z} + \sum_{n=1}^{N_{\text{live}}} \mathcal{L}(x_n) w_{i+1} / N_{\text{live}}$.

Compute the posterior probability for each individual sample $p_i = L_i w_i / \mathcal{Z}$.

cause the dominant source of uncertainty in the final computed evidence \mathcal{Z} . This uncertainty, fortunately, can be estimated easily. We recall below the error estimation scheme presented in [42] using the entropy of the prior volumes. This approach is highly efficient since it does not require any additional sampling.

Let $\mathcal{P}(\xi) = \mathcal{L}(\xi) / \mathcal{Z}$ be the posterior distribution regarding the prior volume ξ . Then the negative relative entropy H can be defined as

$$(3.11) \quad H = \int \mathcal{P}(\xi) \log[\mathcal{P}(\xi)] d\xi \approx \sum_{i=1}^N \frac{L_i w_i}{\mathcal{Z}} \log \left(\frac{L_i}{\mathcal{Z}} \right),$$

which can be computed directly from the obtained likelihoods $\{L_i\}$, weights $\{w_i\}$ and the evidence \mathcal{Z} . Following [42], the standard deviation of the uncertainty of $\log \mathcal{Z}$ using the nested sampling algorithm reads $\sqrt{H/N_{\text{live}}}$, i.e.,

$$(3.12) \quad \log \mathcal{Z} = \log \left(\sum_{i=1}^N L_i w_i \right) \pm \sqrt{\frac{H}{N_{\text{live}}}}.$$

4. Proximal nested sampling framework. The main difficulty in applying nested sampling to large inverse problems, particularly imaging problems, is to efficiently simulate from the prior distribution subject to a hard likelihood constraint. More precisely, at iteration i , the samples from the prior are constrained to the region Ω_{L_i} defined by the likelihood level-set corresponding to L_i (i.e. where a new sample must have a likelihood value greater than L_i at iteration i).

In this section we present our proposed *proximal nested sampling* method to address this challenging constrained sampling problem. Moreover, the proximal nature of the sampling method ensures that non-differentiable distributions, such as popular sparsity-promoting priors involving the ℓ_1 norm, are supported. This section presents the methodology of proximal nested sampling for arbitrary log-concave distributions of the form (2.7). Explicit forms of

proximal nested sampling for common choices of priors and likelihoods in imaging sciences are presented in Section 5.

4.1. General constrained sampling problem. Following (2.7) and adopting the notation of Section 3, assume that the prior and the likelihood are of the form $\pi(x) = \exp(-f(x))$ and $\mathcal{L}(x) = \exp(-g(x))$, where f and g are convex l.s.c. (lower semicontinuous) functions on Ω .

We consider sampling from the prior $\pi(x)$, such that $\mathcal{L}(x) > L^*$ for some generic likelihood value $L^* > 0$. Let $\iota_{L^*}(x)$ and $\chi_{L^*}(x)$ be the indicator function and characteristic function, respectively, defined as

$$(4.1) \quad \iota_{L^*}(x) = \begin{cases} 1, & \mathcal{L}(x) > L^*, \\ 0, & \text{otherwise,} \end{cases} \quad \text{and} \quad \chi_{L^*}(x) = \begin{cases} 0, & \mathcal{L}(x) > L^*, \\ +\infty, & \text{otherwise.} \end{cases}$$

Since \log is monotonic, $\mathcal{L}(x) > L^*$ is equivalent to $g(x) < \tau$, where

$$(4.2) \quad \tau = -\log L^*.$$

Let $\mathcal{B}_\tau := \{x | g(x) < \tau\}$. Then it is apparent that $\chi_{L^*}(x)$, as a constraint for x , is equivalent to $\chi_{\mathcal{B}_\tau}(x)$, where

$$(4.3) \quad \chi_{\mathcal{B}_\tau}(x) = \begin{cases} 0, & x \in \mathcal{B}_\tau, \\ +\infty, & \text{otherwise.} \end{cases}$$

Let $\pi_{L^*}(x) = \pi(x)\iota_{L^*}(x)$ represent the prior distribution with the hard likelihood constraint $\mathcal{L}(x) > L^*$. Since $\iota_{L^*}(x) = \exp(-\chi_{L^*}(x))$, then we have

$$(4.4) \quad \begin{aligned} \pi_{L^*}(x) &= \pi(x)\iota_{L^*}(x) \\ &= \exp(-f(x))\exp(-\chi_{L^*}(x)) \\ &= \exp(-[f(x) + \chi_{L^*}(x)]) \\ &= \exp(-[f(x) + \chi_{\mathcal{B}_\tau}(x)]). \end{aligned}$$

Note that taking logarithm of $\pi_{L^*}(x)$ reads

$$(4.5) \quad -\log \pi_{L^*}(x) = f(x) + \chi_{\mathcal{B}_\tau}(x).$$

In the following section we introduce our proximal nested sampling algorithm for parameter x to sample from the constrained prior distribution $\exp(-[f(x) + \chi_{\mathcal{B}_\tau}(x)])$.

4.2. Drawing a sample from the constrained prior. Sampling distributions over Ω is usually challenging because of the dimensionality involved. Sampling from the constrained prior (4.5) is particularly difficult because of the hard constraint that $x \in \mathcal{B}_\tau$, encoded in the characteristic function $\chi_{\mathcal{B}_\tau}(x)$. Sampling is further complicated if the log-prior $f(x)$ is not Lipschitz differentiable over Ω (e.g. for non-differentiable sparsity-promoting priors), since high-dimensional sampling methods rely heavily on gradient information. To circumvent these issues we adopt a proximal MCMC approach, which is particularly suitable for high-dimensional distributions that are log-concave but not smooth. More precisely, in a

manner akin to [12], we use the unadjusted Langevin algorithm (ULA) MCMC sampling strategy combined with Moreau-Yosida approximations of non-differential terms, followed by Metropolis Hastings correction step to control the approximations made, as described in [33].

Using the ULA iterative formula, for each given τ (recall that τ corresponds to a likelihood value L^* by $\tau = -\log L^*$; see (4.2)), we can generate the following Markov chain

$$(4.6) \quad x^{(k+1)} = x^{(k)} - \frac{\delta}{2} \nabla [f(x^{(k)}) + \chi_{\mathcal{B}_\tau}(x^{(k)})] + \sqrt{\delta} w^{(k+1)},$$

where $\delta > 0$ is the step size and $w^{k+1} \sim \mathcal{N}(0, \mathbf{1}_K)$ (a K -sequence of standard Gaussian random variables).

The non-differentiable characteristic function $\chi_{\mathcal{B}_\tau}(x)$ can be approximated by its Moreau-Yosida envelope $\chi_{\mathcal{B}_\tau}^\lambda(x)$, with approximation controlled by $\lambda > 0$. It is straightforward to show that

$$(4.7) \quad \chi_{\mathcal{B}_\tau}^\lambda(x) = \frac{1}{2\lambda} \|x - x^*\|_2^2,$$

where x^* is the closest point in \mathcal{B}_τ to x , given by the projection of x onto \mathcal{B}_τ , i.e. $x^* = \text{proj}_{\mathcal{B}_\tau}(x) = \text{prox}_{\chi_{\mathcal{B}_\tau}}(x)$. Critically, the λ -Moreau-Yosida envelope is $\frac{1}{\lambda}$ -Lipschitz differentiable. Its gradient can be calculated directly from (4.7) or by noting (2.6), yielding

$$(4.8) \quad \nabla \chi_{\mathcal{B}_\tau}^\lambda(x) = (x - x^*)/\lambda = (x - \text{prox}_{\chi_{\mathcal{B}_\tau}}(x))/\lambda.$$

Replacing the characteristic function by its Moreau-Yosida approximation in (4.6), and noting the gradient (4.8), yields

$$(4.9) \quad x^{(k+1)} = x^{(k)} - \frac{\delta}{2} \nabla f(x^{(k)}) - \frac{\delta}{2\lambda} [x^{(k)} - \text{prox}_{\chi_{\mathcal{B}_\tau}}(x^{(k)})] + \sqrt{\delta} w^{(k+1)}.$$

When $f(x)$ is differentiable its gradient can be computed directly (we consider the case where $f(x)$ is non-differentiable shortly). For differential log-priors $f(x)$, (4.9) provides the general strategy for sampling from the prior subject to the hard likelihood constraint (with a subsequent Metropolis-Hastings step as discussed below).

If the sample $x^{(k)}$ is already in \mathcal{B}_τ , i.e. $x \in \mathcal{B}_\tau$, the term $[x^{(k)} - \text{prox}_{\chi_{\mathcal{B}_\tau}}^\lambda(x^{(k)})]$ disappears and the Markov chain iteration simply involves taking a noisy step to descent the gradient. In contrast, if $x^{(k)}$ is not in \mathcal{B}_τ , i.e. $x \notin \mathcal{B}_\tau$, then a step is also taken in the direction $[-[x^{(k)} - \text{prox}_{\chi_{\mathcal{B}_\tau}}^\lambda(x^{(k)})]]$, which acts to move the next iteration in the Markov chain in the direction of the projection of $x^{(k)}$ onto the convex set \mathcal{B}_τ . This term therefore acts to push the Markov chain back into the constraint set \mathcal{B}_τ if it wanders outside of it, although due to the Moreau-Yosida approximation of $\chi_{\mathcal{B}_\tau}$ it does not guarantee the constraint is satisfied (the subsequent Metropolis-Hastings step does guarantee the hard likelihood constraint is satisfied as discussed below).

When $f(x)$ is non-differentiable, it may be approximated by its differentiable Moreau-Yosida envelope $f^\lambda(x)$. By noting (2.6), the gradient of the term involving the sum of the two Moreau-Yosida approximations then reads

$$(4.10) \quad \nabla(f^\lambda(x) + \chi_{\mathcal{B}_\tau}^\lambda(x)) = (x - \text{prox}_f^\lambda(x))/\lambda + (x - \text{prox}_{\chi_{\mathcal{B}_\tau}}(x))/\lambda.$$

Here we have used the same regularisation parameter $\lambda > 0$ for both approximations for notational brevity, although clearly different parameters can be considered for $f^\lambda(x)$ and $\chi_{\mathcal{B}_\tau}^\lambda(x)$ if desired.

Replacing in (4.6) both $f(x)$ and $\chi_{\mathcal{B}_\tau}(x)$ by their Moreau-Yosida approximations, and noting the gradient (4.10), yields

$$(4.11) \quad x^{(k+1)} = (1 - \frac{\delta}{\lambda})x^{(k)} + \frac{\delta}{2\lambda} \text{prox}_f^\lambda(x^{(k)}) + \frac{\delta}{2\lambda} \text{prox}_{\chi_{\mathcal{B}_\tau}}(x^{(k)}) + \sqrt{\delta}w^{(k+1)}.$$

For non-differentiable log-concave priors, (4.11) provides the general strategy for sampling from the prior subject to the hard likelihood constraint.

To summarise, given a proper initial sample, say $x^{(0)}$, we generate a Markov chain by iteratively applying the Markov kernel (4.9) if f is Lipschitz differentiable or the regularised surrogate (4.11) if it is not, which allows drawing samples from the prior that are likely to be within the likelihood iso-contour L^* . This is the main challenge in nested sampling.

The Markov chains generated by ULA-type kernels exhibit some bias resulting from the discretisation of the Langevin stochastic differential equation and from the use of Moreau-Yosida regularisations. This bias can be asymptotically removed by introducing a Metropolis-Hastings correction step to ensure convergence to the required target density. In detail, at each iteration, a new candidate x' generated using formula (4.9) or (4.11) is then accepted with probability

$$(4.12) \quad \min \left\{ 1, \frac{q(x^{(k)}|x')\pi_{L^*}(x')}{q(x'|x^{(k)})\pi_{L^*}(x^{(k)})} \right\},$$

where $q(\cdot|\cdot)$ is a transition kernel, which we define by a Gaussian related to the ULA random component (following [33]), i.e.,

$$(4.13) \quad q(x'|x^{(k)}) \sim \exp \left(-\frac{(x' - x^{(k)} - \frac{\delta}{2}\nabla \log \pi_{L^*}(x^{(k)}))^2}{2\delta} \right).$$

If the candidate sample x' is outside of \mathcal{B}_τ , i.e. $x' \notin \mathcal{B}_\tau$, then $\pi_{L^*}(x') = 0$ and according to the Metropolis-Hastings update the candidate will not be accepted, ensuring the hard likelihood constraint is satisfied.

We summarise our proximal technique to draw an individual sample from the prior under the hard likelihood constraint in Algorithm 4.1.

4.3. Initialisation with samples from the unconstrained prior. The initialisation of the nested sampling method is to draw N_{live} samples $\{x_n\}_{n=1}^{N_{\text{live}}}$ from the prior distribution $\pi(x)$ in the prior space Ω . If the log-prior $f(x)$ is differentiable this may be applied trivially with the ULA iterative formula. Otherwise $f(x)$ may again be approximated by its Moreau-Yosida envelope and samples from the prior can be generated by the iterative formula

$$(4.14) \quad x^{(k+1)} = (1 - \frac{\delta}{2\lambda})x^{(k)} + \frac{\delta}{2\lambda} \text{prox}_f^\lambda(x^{(k)}) + \sqrt{\delta}w^{(k+1)}.$$

To draw N_{live} samples from the prior, it is necessary to first discard initial samples generated before converging on the target prior distribution. Initial samples corresponding to a number

Algorithm 4.1 Proximal individual sample draw algorithm

 ProxSampleDraw($x^{(0)}$, L^*)

Initialization: $k = 0$, K_{gap} .

Input: $x^{(0)}$, L^* (starting point of Markov chain and likelihood threshold).

Output: Individual sample x_{new} fulfilling constraint $\mathcal{L}(x) > L^*$.

 Compute $\tau = -\log L^*$.

for $k = 1, \dots$

 - Compute $x^{(k)}$ using the iterative formula (4.9) if f is differentiable; otherwise (4.11).

- Metropolis-Hastings step following (4.12) to remove the estimation bias.

if $\mathcal{L}(x^{(k)}) > L^*$ and $k \geq K_{\text{gap}}$

break.

end if
end for

 Set $x_{\text{new}} = x^{(k)}$.

of burn-in iterations, say K_{burn} , are discarded. Due to correlations between samples and the algorithm's memory footprint, the chain is thinned by discarding a number of intermediate iterations between samples (the chain's thinning factor), say $(K_{\text{gap}} - 1)$. That is, only the K_{gap} -th sample generated by the iterative formula is kept. Only 1-in- K_{gap} samples are stored when $k > K_{\text{burn}}$ and $\text{mod}(k - K_{\text{burn}}, K_{\text{gap}}) = 0$, where $\text{mod}(\cdot, \cdot)$ represents modulus after division. A Metropolis-Hastings step can also be introduced here to remove the estimation bias. We summarise the technique for drawing N_{live} live samples from the prior in Algorithm 4.2.

Algorithm 4.2 Proximal algorithm of drawing live samples (from prior)

Initialization: N_{live} , K_{burn} , K_{gap} , and $x^{(0)}$.

Output: N_{live} live samples $\{x_n\}_{n=1}^{N_{\text{live}}}$ (draw from the prior with no constraint).

for $k = 1, \dots, K_{\text{burn}}$

 - Compute $x^{(k)}$ using the iterative formula (4.14).

end for
 $n = 1$;

for $k = K_{\text{burn}} + 1, \dots, K_{\text{burn}} + N_{\text{live}}K_{\text{gap}}$

 - Compute $x^{(k)}$ using the iterative formula (4.14).

- Metropolis-Hastings step to remove the estimation bias.

if $\text{mod}(k - K_{\text{burn}}, K_{\text{gap}}) = 0$
 $x_n = x^{(k)}$; $n = n + 1$.

end if
end for

4.4. Proximal nested sampling algorithm. After embedding Algorithms 4.1 and 4.2 into Algorithm 3.1 (i.e., the standard nested sampling algorithm), we obtain our proposed proximal nested sampling algorithm, which is summarised in Algorithm 4.3. Recall that Algorithm 4.1 generates a new single sample from the prior subject to the hard likelihood constraint, which is

used to replace the sample with the lowest likelihood value in the live sample set. We suggest using a sample randomly selected from the live sample set as a starting point for Algorithm 4.1.

So far we have presented the proximal nested sampling framework in its most general form for arbitrary log-concave distributions, which is based on the iterative formula (4.9) or (4.11) to sample from the constrained prior. These iterative formula involve computing proximal operators related to the log-prior and likelihood constraint, which we have not yet considered in further detail. In principle computing proximal operators involves solving a minimisation problem, although in many scenarios this can be solved analytically or otherwise efficient iterative algorithms can be used. In the following section we consider explicit forms of proximal nested sampling for common forms of the prior and likelihood, outlining explicitly how the required proximal operators can be computed.

Algorithm 4.3 Proximal nested sampling algorithm

Initialization: Data Y . Set $\mathcal{Z} = 0$, $\xi_0 = 1$ and $i = 0$. Using Algorithm 4.2 to draw N_{live} samples $\{x_n\}_{n=1}^{N_{\text{live}}}$ from the prior distribution $\pi(x)$ in the prior space Ω .

Output: Evidence \mathcal{Z} and posterior probabilities $\{p_i\}$.

for $i = 1, \dots$, until the stopping criterion reached

- Find the lowest likelihood, say L_i , in the set of live samples.
- Compute weight $w_i = (\xi_{i-1} - \xi_{i+1})/2$, where $\xi_i = \exp(-i/N_{\text{live}})$.
- Update evidence by $\mathcal{Z} = \mathcal{Z} + L_i w_i$.
- Randomly select a sample, say $x^{(0)}$, from the set of live samples.
- Use Algorithm 4.1 to draw a new sample $x_{\text{new}} = \text{ProxSampleDraw}(x^{(0)}, L_i)$ from the prior distribution $\pi(x)$ in the restricted parameter space Ω_{L_i} , and replace the individual sample $x_{i,\text{low}}$ by the newly drawn sample x_{new} .

end for

Update the evidence by $\mathcal{Z} = \mathcal{Z} + \sum_{n=1}^{N_{\text{live}}} \mathcal{L}(x_n) w_{i+1} / N_{\text{live}}$.

Compute the posterior probability for each individual sample $p_i = L_i w_i / \mathcal{Z}$.

5. Explicit forms of proximal nested sampling. In the general proximal nested sampling framework presented in Section 4 we considered arbitrary log-concave terms for the prior and likelihood and did not consider further how to compute the proximal operators related to those terms. We now exemplify our proposed proximal nested sampling framework with explicit forms for common priors and likelihoods used in high-dimensional signal and image processing problems. In particular, we outline explicitly how to compute the required proximal operators.

For illustration, we focus on sparsity-promoting priors corresponding to $f(x) = \mu \|\Psi^\dagger x\|_1$, where $\Psi^\dagger \in \mathbb{C}^{p \times d}$ represents a sparsifying transform, and Gaussian likelihoods corresponding to $g(x) = \|y - \Phi x\|_2^2 / 2\sigma^2$, where $y \in \mathbb{C}^m$ denotes measured data, $x \in \mathbb{R}^d$ the underlying parameters, and $\Phi \in \mathbb{C}^{m \times d}$ the measurement operator (model), although other common priors are also considered. For simplicity, although not essential, we assume Ψ is an orthonormal transformation, i.e., $\Psi^\dagger \Psi = \Psi \Psi^\dagger = I$.

From the iterative forms given in (4.9), (4.11) and (4.14), on which our proximal nested

sampling framework is based, it is necessary to compute two proximal operators: $\text{prox}_f^\lambda(x)$ and $\text{prox}_{\chi_{\mathcal{B}_\tau}}(x)$, related to the prior and likelihood, respectively (recall that the definition of $\chi_{\mathcal{B}_\tau}$ is related to likelihood function g ; see (4.3)). In the following we calculate these two proximal operators for explicit expressions of $f(x)$ and $g(x)$ and show the corresponding explicit forms of the iterative formulas of (4.9), (4.11) and (4.14).

5.1. Proximal operator for the prior. When $f(x)$ represents a flat prior or $f(x) = \mu\|\Psi^\dagger x\|_2^2$ (Gaussian prior) it is differentiable with gradient

$$(5.1) \quad \nabla f(x) = 0 \quad \text{or} \quad \nabla f(x) = 2\mu\Psi\Psi^\dagger x = 2\mu x,$$

respectively (here we use $\Psi\Psi^\dagger = I$). Obviously, there is no need to use the Moreau-Yosida envelope $\nabla f^\lambda(x)$ to approximate $\nabla f(x)$ when $f(x)$ is differentiable.

When $f(x)$ represents a sparsity-promoting Laplacian-type prior $f(x) = \mu\|\Psi^\dagger x\|_1$, $\forall x' \in \mathbb{R}^d$, we have

$$(5.2) \quad \begin{aligned} \text{prox}_f^\lambda(x') &= \underset{x \in \mathbb{R}^d}{\operatorname{argmin}} \left\{ \mu\|\Psi^\dagger x\|_1 + \|x - x'\|_2^2/2\lambda \right\} \\ &= x' + \Psi \left(\text{prox}_{\|\cdot\|_1}^{\lambda\mu}(\Psi^\dagger x') - \Psi^\dagger x' \right) \\ &= x' + \Psi \left(\text{soft}_{\lambda\mu}(\Psi^\dagger x') - \Psi^\dagger x' \right), \end{aligned}$$

where the second line follows by standard properties of the proximal operator [11] and where $\text{soft}_\lambda(x) = (\text{soft}_\lambda(x_1), \text{soft}_\lambda(x_2), \dots)$ is the soft-thresholding operator defined by

$$(5.3) \quad \text{soft}_\lambda(x_i) = \begin{cases} 0, & |x_i| < \lambda, \\ x_i(|x_i| - \lambda)/|x_i|, & \text{otherwise.} \end{cases}$$

5.2. Proximal operator for the likelihood. Consider the Gaussian likelihood corresponding to $g(x) = \|y - \Phi x\|_2^2/2\sigma^2$. Recall that $\chi_{\mathcal{B}_\tau}(x) = 0$ if $x \in \{x | g(x) < \tau\}$ and otherwise $\chi_{\mathcal{B}_\tau}(x) = +\infty$. We are to solve

$$(5.4) \quad \begin{aligned} \text{prox}_{\chi_{\mathcal{B}_\tau}}^\lambda(x') &= \underset{x \in \mathbb{R}^d}{\operatorname{argmin}} \left\{ \chi_{\mathcal{B}_\tau}(x) + \|x - x'\|_2^2/2\lambda \right\} \\ &= \underset{x \in \mathbb{R}^d}{\operatorname{argmin}} \left\{ \chi_{\mathcal{B}_\tau}(x) + \|x - x'\|_2^2 \right\} \\ &= \text{proj}_{\chi_{\mathcal{B}_\tau}}(x'), \end{aligned}$$

which is a projection onto set \mathcal{B}_τ .

For the case where the measurement operator is the identity, $\Phi = I$, (e.g. denoising problems) then problem (5.4) is the projection onto the ℓ_2 ball with radius $\sqrt{2\tau\sigma^2}$. In this case the proximal (projection) operator has closed-form solution

$$(5.5) \quad \text{proj}_{\chi_{\mathcal{B}_\tau}}(x) = \begin{cases} x, & \text{if } x \in \mathcal{B}_\tau, \\ \frac{x-y}{\|x-y\|_2} \sqrt{2\tau\sigma^2} + y, & \text{otherwise.} \end{cases}$$

For the case where the measurement operator is not the identity, $\Phi \neq I$, problem (5.4) is equivalent to finding an $x \in \mathbb{R}^d$ satisfying

$$(5.6) \quad \min_{x \in \mathbb{R}^d} \{ \chi_{\mathcal{B}'_{\tau'}}(u) + \|x - x'\|_2^2/2 \}, \quad \text{s.t. } u = \Phi x,$$

where $\mathcal{B}'_{\tau} := \{z \mid \|y - z\|_2^2 < \tau\}$ and $\tau' = 2\tau\sigma^2$. Minimisation problem (5.6) can be solved by a variety of different optimisation methods, e.g. by the alternating direction method of multipliers (ADMM) and primal-dual algorithms (see e.g. [32] and references therein for more details). In the following we present detailed procedures for using the ADMM and primal-dual algorithms to solve problem (5.6).

5.2.1. Computation using ADMM method. Firstly, the augmented Lagrangian of the minimisation problem (5.6) can be represented as

$$(5.7) \quad \Lambda(x, u, z) := \chi_{\mathcal{B}'_{\tau'}}(u) + \frac{1}{2}\|x - x'\|_2^2 + \beta z^\dagger(u - \Phi x) + \frac{\beta}{2}\|u - \Phi x\|_2^2,$$

for dual variable z and penalty parameter $\beta > 0$. Starting from an initialisation $x^{(0)}, z^{(0)}$, the augmented Lagrangian of (5.7) can be minimised with respect to variables u and x alternatively, while updating the dual value z using the dual ascent method to ensure the constraint $u = \Phi x$ is satisfied for the final solution, i.e.

$$(5.8) \quad u^{(i)} = \underset{u \in \mathbb{C}^m}{\operatorname{argmin}} \Lambda(x^{(i)}, u, z^{(i)}),$$

$$(5.9) \quad x^{(i+1)} = \underset{x \in \mathbb{R}^d}{\operatorname{argmin}} \Lambda(x, u^{(i)}, z^{(i)}),$$

$$(5.10) \quad z^{(i+1)} = z^{(i)} + u^{(i)} - \Phi x^{(i+1)},$$

which can be rewritten as the following explicit iterative scheme

$$(5.11) \quad u^{(i)} = \underset{u \in \mathbb{C}^M}{\operatorname{argmin}} \left\{ \chi_{\mathcal{B}'_{\tau'}}(u) + \frac{\beta}{2}\|u - \Phi x^{(i)} + z^{(i)}\|_2^2 \right\},$$

$$(5.12) \quad x^{(i+1)} = \underset{x \in \mathbb{R}^D}{\operatorname{argmin}} \left\{ \frac{1}{2}\|x - x'\|_2^2 + \frac{\beta}{2}\|u^{(i)} - \Phi x + z^{(i)}\|_2^2 \right\},$$

$$(5.13) \quad z^{(i+1)} = z^{(i)} + u^{(i)} - \Phi x^{(i+1)}.$$

The solution to problem (5.11) has a closed-form expression since it is the projection onto a scaled and shifted ℓ_2 ball, i.e.,

$$(5.14) \quad u^{(i)} = \begin{cases} \Phi x^{(i)} - z^{(i)}, & \text{if } \Phi x^{(i)} - z^{(i)} \in \mathcal{B}'_{\tau'}, \\ \frac{\Phi x^{(i)} - z^{(i)} - Y}{\|\Phi x^{(i)} - z^{(i)} - Y\|_2} \sqrt{2\tau\sigma^2} + Y, & \text{otherwise.} \end{cases}$$

Problem (5.12) is differentiable and so can be solved by gradient descent. It is straightforward to show that this problem is equivalent to solving the linear system w.r.t. x

$$(5.15) \quad (\beta\Phi^\dagger\Phi + I)x = x' + \beta\Phi^\dagger(u^{(i)} + z^{(i)}),$$

which can be solved by using iterative methods, with $(\beta\Phi^\dagger\Phi + I)$ positive definite.

The pseudo code to compute the proximal operator, $\text{prox}_{\chi_{\mathcal{B}_\tau}}(x)$, using ADMM is summarised in Algorithm 5.1. Various stopping criteria can be considered, such as a maximum iteration number or the relative error of solutions at two consecutive iterations, i.e., $\|x^{(i+1)} - x^{(i)}\|_2/\|x^{(i)}\|_2$.

Algorithm 5.1 ADMM for proximal operator associated with the likelihood

Initialization: $x^{(0)}, z^{(0)}$.

Input: x, L^*

Output: x^* (the value of $\text{prox}_{\chi_{\mathcal{B}_\tau}}(x)$).

Compute $\tau = -\log L^*$, and form $\chi_{\mathcal{B}_\tau}$.

for $i = 0, \dots$, until the stopping criterion reached

- Compute $u^{(i)}$ by (5.14);
- Compute $x^{(i+1)}$ by solving (5.15);
- Update $z^{(i+1)}$ by (5.13).

end for

Set $x^* = x^{(i+1)}$.

5.2.2. Computation using primal-dual method. Alternatively, problem (5.4) can be solving using a primal-dual method. Note that the problem can be rewritten as

$$(5.16) \quad \min_{x \in \mathbb{R}^d} \left\{ \chi_{\mathcal{B}'_\tau}(\Phi x) + \|x - x'\|_2^2/2 \right\},$$

which is equivalent to the saddle-point problem

$$(5.17) \quad \min_{x \in \mathbb{R}^d} \max_{z \in \mathbb{C}^K} \left\{ z^\dagger \Phi x - \chi_{\mathcal{B}'_\tau}^*(z) + \|x - x'\|_2^2/2 \right\},$$

where $\chi_{\mathcal{B}'_\tau}^*$ is the convex conjugate of $\chi_{\mathcal{B}'_\tau}$. The saddle-point problem (5.17) can be solved by alternatively optimising with respect to the primal variable x and the dual variable z . Considering a proximal forward-background step for each alternate optimisation, first for the dual variable z followed by the primal variable x , leads to the following iterative scheme

$$(5.18) \quad z^{(i+1)} = \text{prox}_{\chi_{\mathcal{B}'_\tau}^*}(z^{(i)} + \delta_1 \Phi \bar{x}^{(i)}),$$

$$(5.19) \quad x^{(i+1)} = \text{prox}_h(x^{(i)} - \delta_2 \Phi^\dagger z^{(i+1)}),$$

$$(5.20) \quad \bar{x}^{(i+1)} = x^{(i+1)} + \delta_3(x^{(i+1)} - x^{(i)}),$$

where $h(x) = \|x - x'\|_2^2/2$, and δ_k , for $k = 1, 2, 3$, are algorithm step size parameters. We next consider how to solve problem (5.18) and (5.19) explicitly.

Problem (5.18) can be solved by

$$(5.21) \quad \begin{aligned} z^{(i+1)} &= \text{prox}_{\chi_{\mathcal{B}'_\tau}^*}(z^{(i)} + \delta_1 \Phi \bar{x}^{(i)}) \\ &= z^{(i)} + \delta_1 \Phi \bar{x}^{(i)} - \text{prox}_{\chi_{\mathcal{B}'_\tau}}(z^{(i)} + \delta_1 \Phi \bar{x}^{(i)}), \end{aligned}$$

where we have noted the relationship between the proximal operator of the convex conjugate of a function given by (2.4). Since $\mathcal{B}'_{\tau'}$ is an ℓ_2 ball, the proximal operator in (5.21) has the closed-form expression

$$(5.22) \quad \text{prox}_{\chi_{\mathcal{B}'_{\tau'}}}(z) = \text{proj}_{\mathcal{B}'_{\tau'}}(z) = \begin{cases} z, & \text{if } z \in \mathcal{B}'_{\tau'}, \\ \frac{z-y}{\|z-y\|_2} \sqrt{2\tau\sigma^2} + y, & \text{otherwise.} \end{cases}$$

Problem (5.19) is to solve

$$(5.23) \quad x^{(i+1)} = \underset{x \in \mathbb{R}^d}{\operatorname{argmin}} \left\{ \|x - x'\|_2^2 + \|x - (x^{(i)} - \delta_2 \Phi^\dagger z^{(i+1)})\|_2^2 \right\},$$

which involves a differentiable objective function and so can be solved analytically, yielding the closed-form solution

$$(5.24) \quad x^{(i+1)} = (x' + x^{(i)} - \delta_2 \Phi^\dagger z^{(i+1)})/2.$$

The pseudo code to compute the proximal operator, $\text{prox}_{\chi_{\mathcal{B}_\tau}}^\lambda(x)$, using the primal-dual method is summarised in Algorithm 5.2. The same stopping criterion as for ADMM in Algorithm 5.1 can also be used for Algorithm 5.2.

Note that the main difference between the primal-dual method and ADMM is that the primal-dual method does not need to solve the linear system in (5.15). Therefore, the primal-dual method is typically more efficient computationally and is the approach used in the numerical experiments that follow. However, there are specific problems for which the linear system in (5.15) admits a computationally efficient solution and where the ADMM method might be more appropriate.

Algorithm 5.2 Primal-dual method for proximal operator associated with the likelihood

Initialization: $x^{(0)}, \bar{x}^{(0)}, z^{(0)}$.

Input: x, L^*

Output: x^* (the value of $\text{prox}_{\chi_{\mathcal{B}_\tau}}(x)$).

Compute $\tau = -\log L^*$, and form $\chi_{\mathcal{B}_\tau}$.

for $i = 0, \dots$, until the stopping criterion reached

- Compute $z^{(i+1)}$ by (5.21);
- Compute $x^{(i+1)}$ by solving (5.24);
- Update $\bar{x}^{(i+1)}$ by (5.20).

end for

Set $x^* = x^{(i+1)}$.

5.3. Explicit iterative formula for drawing samples. We are now in a position to outline the explicit iterative formulas to draw samples for a variety of common priors using our proximal nested sampling method.

The explicit representations of the iterative equations (4.9) (for differentiable $f(x)$) and (4.11) (for non-differentiable $f(x)$), which are used in Algorithm 4.1 to draw an individual

sample from the prior under the hard likelihood constraint, for uniform, Gaussian and Laplacian priors, i.e. $f(x)$ constant, $f(x) = \mu\|\Psi^\dagger x\|_2^2$ and $f(x) = \mu\|\Psi^\dagger x\|_1$, respectively, are

$$(5.25) \quad x^{(k+1)} = (1 - \frac{\delta}{2\lambda})x^{(k)} + \frac{\delta}{2\lambda}x^{*(k)} + \sqrt{\delta}w^{(k+1)},$$

$$(5.26) \quad x^{(k+1)} = (1 - \frac{\delta}{2\lambda} - \delta\mu)x^{(k)} + \frac{\delta}{2\lambda}x^{*(k)} + \sqrt{\delta}w^{(k+1)},$$

$$(5.27) \quad x^{(k+1)} = (1 - \frac{\delta}{2\lambda})x^{(k)} + \frac{\delta}{2\lambda}\Psi(\text{soft}_{\lambda\mu}(\Psi^\dagger x^{(k)}) - \Psi^\dagger x^{(k)}) + \frac{\delta}{2\lambda}x^{*(k)} + \sqrt{\delta}w^{(k+1)},$$

where $x^{*(k)} = \text{prox}_{\chi_{\mathcal{B}_\tau}}(x^{(k)})$ is obtained using Algorithm 5.1 or 5.2.

Correspondingly, the explicit representations of equation (4.14), which is used in Algorithm 4.2 to draw N_{live} initial live samples from the prior distribution $\pi(x)$ in the prior space Ω , are, respectively,

$$(5.28) \quad x^{(k+1)} = x^{(k)} + \sqrt{\delta}w^{(k+1)},$$

$$(5.29) \quad x^{(k+1)} = (1 - \delta\mu)x^{(k)} + \sqrt{\delta}w^{(k+1)},$$

$$(5.30) \quad x^{(k+1)} = x^{(k)} + \frac{\delta}{2\lambda}\Psi(\text{soft}_{\lambda\mu}(\Psi^\dagger x^{(k)}) - \Psi^\dagger x^{(k)}) + \sqrt{\delta}w^{(k+1)}.$$

6. Numerical experiments. In this section we validate our proposed proximal nested sampling method and demonstrate its utility on a range of illustrative problems.

We first validate our method on a problem with a Gaussian likelihood and Gaussian prior where the value of the marginal likelihood (Bayesian evidence) can be computed analytically. The dimensions of the problem considered range from low to very high, i.e. 2 to 10^6 dimensions.

Following on from this, we demonstrate the effectiveness of the proximal nested sampling method by applying it to two canonical imaging inverse problems, namely image denoising and image reconstruction. In particular, we demonstrate the use of proximal nested sampling for the principled Bayesian model selection of the sparsifying dictionary, the regularisation parameter (i.e. the μ parameter of the prior) and the appropriate measurement operator when it may be misspecified. Furthermore, as mentioned already, as a by-product the samples obtained by nested sampling approaches can also be used to perform posterior inferences. This is critical in imaging problems in order to recover point estimates, e.g. restored images. Moreover, alternative forms of uncertainty quantification can also be considered from other posterior inferences, e.g. variance estimates and posterior credible regions (see, e.g., [4]).

6.1. Implementation and computational resources. To perform the numerical experiments presented subsequently, the proximal nested sampling algorithms developed in this article were implemented in MATLAB in the `proxnest` code.² The numerical experiments performed to compute the marginal likelihood for low-dimensional problems (i.e., dimensions less than 200) were run on a Macbook laptop with an i7 Intel CPU and memory of 16 GB. A high-performance workstation, with 24 CPU cores, x86 64 architecture and 256 GB memory, was used for high-dimensional problems.

²`proxnest` will be made public following the publication of this article. In the interim please contact the authors for access. (A Python implementation is also in development.)

6.2. Validation in high dimensions. We first consider the validation of the proximal nested sampling method. For ease of validation, we consider the prior potential $f(x) = \mu\|\Psi^\dagger x\|_2^2$, with $\mu = 1/2$, $\Psi = I$, and the likelihood potential $g(x) = \|y - \Phi x\|_2^2/2\sigma^2$, with $\sigma = 1$, $\Phi = I$. For this setting, we have a closed-form solution of the marginal likelihood value (see Appendix for further details). Test data $y \in \mathbb{R}^d$ are generated by

$$(6.1) \quad y = x + w,$$

where x is an d -dimensional vector of uniformly distributed random numbers in $[0, 1]^d$, and w is an d -dimensional vector of normally distributed random numbers. Note that the underlying model used to generate the mock data does not match the prior π used here, but that is fine for validation of the calculation of the marginal likelihood. Also, in imaging setting the prior is never perfectly specified. In the following, we consider increasing dimensions from $d = 2$ to $d = 10^6$. We separate the test into three parts: i) small models of dimension from $d = 2$ to $d = 200$, ii) moderately large models of dimension from $d = 2$ to $d = 10^5$, and iii) high dimensional models with $d = 10^6$.

We first test our method for low-dimensional models (i.e., $d < 200$). For our proximal nested sampling method, we use $N_{\text{live}} = 2 \times 10^2$ live samples and $N = 3 \times 10^3$ dead samples, with a thinning factor of 10. We also compare our result with vanilla Monte Carlo (MC) integration where a uniform prior with integrand $f \cdot g$ is utilised, with the number of samples set to 10^5 . Fig. 6.1 presents the results. Our proximal nested sampling method agrees well with the ground truth, whereas simple MC integration can only achieve acceptable results when the dimension is small, say $d < 20$. The computation time for the problem with dimension 200 is approximately one minute.

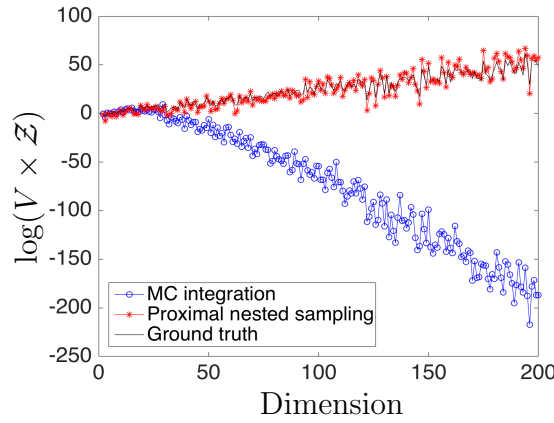


Figure 6.1. Validation of our proximal nested sampling technique (for dimensions 2 to 200) to compute the marginal likelihood (Bayesian evidence) for a scenario where a closed-form solution is accessible. The logarithm of the unnormalised prior volume (V) times the marginal likelihood value (\mathcal{Z}) is plotted against the dimensions of the problem considered. The blue-circle line, red-asterisk line and the black-solid line show the results of MC integration, proximal nested sampling and the ground truth, respectively. We can clearly see that the results computed by proximal nested sampling agree with the ground truth well, whereas the result computed by MC integration with 10^5 samples can only achieve acceptable results when the dimension is below ~ 20 . The computation time for the problem with dimension 200 is approximately one minute.

We now test our proximal nested sampling method for high-dimensional cases. Results for dimensions of y up to 10^5 are given in Figure 6.2, where we set the number of the live samples $N_{\text{live}} = 10^3$ and the number of dead samples $N = 10^4$, with thinning factor 10 (we do not consider direct MC integration any further since it is already shown to fail for dimensions above ~ 20). These results again show that our proximal nested sampling method can achieve results in close agreement with the ground truth. The computation time for the problem with dimension 10^5 is approximately 10 minutes.

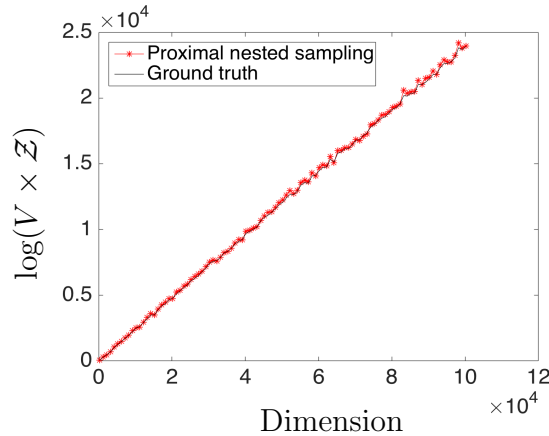


Figure 6.2. Validation of our proximal nested sampling technique (for dimensions up to 10^5) to compute the marginal likelihood (Bayesian evidence) for a scenario where a closed-form solution is accessible. The logarithm of the unnormalised prior volume (V) times the marginal likelihood value (Z) is plotted against the dimensions of the problem considered. The red-asterisk line and the black-solid line show the results of proximal nested sampling and the ground truth, respectively. We can clearly see that the results computed by proximal nested sampling agrees with the ground truth well. The computation time for the problem with dimension 10^5 is approximately 10 minutes.

Finally, we consider dimension 10^6 as an example to show that our proximal nested sampling method can be pushed to dimensions much higher than 10^5 . With the same parameters as that used for dimension 10^5 , ten runs were performed for a 10^6 dimensional setting of the same problem. The logarithm of the ground truth value was calculated to be 2.3850×10^5 . The mean of ten runs of proximal nested sampling was computed to be 2.3851×10^5 , with standard deviation 0.0002×10^5 . The result computed by proximal nested sampling is in excellent agreement with the ground truth. The computation time for each run of the problem with dimension 10^6 is approximately 30 minutes.

6.3. Model selection in image processing. We now illustrate the application of proximal nested sampling for Bayesian model selection in imaging problems. In particular, we focus on two canonical problems, image denoising and image reconstruction, with different likelihoods and priors. We emphasise that Bayesian model selection for these imaging problems is not well addressed by existing techniques due to the high dimensions considered (i.e., higher than 10^5) and the use of general log-concave priors (e.g., like the sparsity promoting Laplace-type priors that include ℓ_1 terms).

The three images in Fig. 6.3 are used in the experiments that follow: Cameraman image,

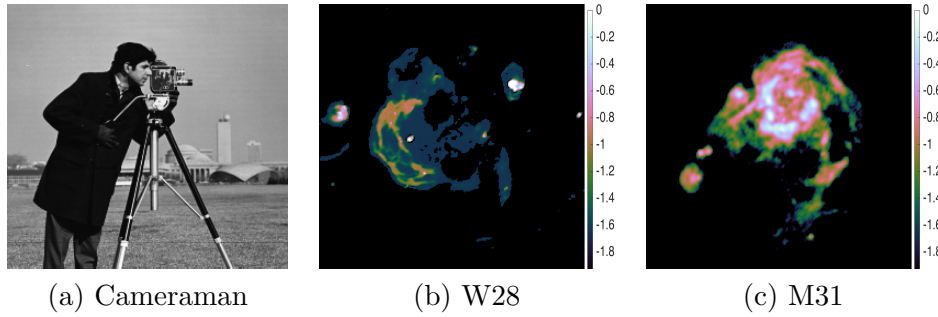


Figure 6.3. Images used to showcase the use of proximal nested sampling for Bayesian model selection in high-dimensional image processing problems. Panel (a): Cameraman grey-scale image; Panels (b)–(c): W28 and M31 radio galaxies normalised to $[0, 1]$ and then shown in \log_{10} scale (i.e. the numeric labels on the colour bar are the logarithms of the image intensity), respectively.

the W28 supernova remnant, and the HI region of the M31 galaxy, all with size of 256×256 pixels and with intensities in the range $[0, 255]$. Sparsity-promoting priors (which are not smooth) and Gaussian likelihoods are considered in the following experiments, formed as $f(x) = \mu \|\Psi^\dagger x\|_1$ and $g(x) = \|y - \Phi x\|_2^2 / 2\sigma^2$, respectively, where μ , Ψ and Φ are set to different forms for model selection purposes.

6.3.1. Prior model selection in image denoising: dictionary selection. For a standard denoising problem we apply proximal nested sampling to select the dictionary Ψ used for the sparsifying transform. The noisy image y is generated by $y = x + w$, where x is the ground truth clean image and w is Gaussian noise with zero mean and standard deviation $\sigma = \|x\|_\infty 10^{-\text{SNR}/20}$, where $\|\cdot\|_\infty$ is the infinity norm, and the input signal-to-noise ratio (SNR) is set to 20. Set $\Phi = I$ in the likelihood $g(x) = \|y - \Phi x\|_2^2 / 2\sigma^2$ (i.e., $g(x) = \|y - x\|_2^2 / 2\sigma^2$). We then investigate the influence of different choices for Ψ in the prior term $f(x) = \mu \|\Psi^\dagger x\|_1$, with $\mu = 10^5$. Specifically, three forms of Ψ are considered, namely the identity (I), Daubechies 2 wavelets (DB2), and Daubechies 8 wavelets (DB8). For the proximal nested sampling method, the number of the live samples N_{live} and dead samples N is respectively set to 2×10^3 , and 4×10^4 with thinning factor 10^2 , which is sufficient to ensure convergence.

Fig. 6.4 presents the posterior means recovered (i.e. the reconstructed images) for the three dictionaries considered, i.e. for $\Psi = \{I, \text{DB2}, \text{DB8}\}$. It is clear that the reconstructed images corresponding to $\Psi = \text{DB2}$ and DB8 are significantly better than that for $\Psi = I$. Moreover, while the difference between the reconstructed images of the models for $\Psi = \text{DB2}$ and DB8 is small, by eye the image recovered with DB2 may be judged slightly superior.

Table 6.1 presents the calculated marginal likelihood values³ for the different sparsifying transforms Ψ selected for the prior. The root mean square error (RMSE) is also given, where the RMSE gauges the difference between the posterior mean image and the ground truth image. Note that the RMSE cannot normally be computed in practical problems since the ground truth is not known. Since for these experiments we know the ground truth the RMSE is a useful measure for comparison purposes.

³The value of the log marginal likelihoods computed is low (in other words, its absolute value is very high) since the problems we consider are extremely high-dimensional.

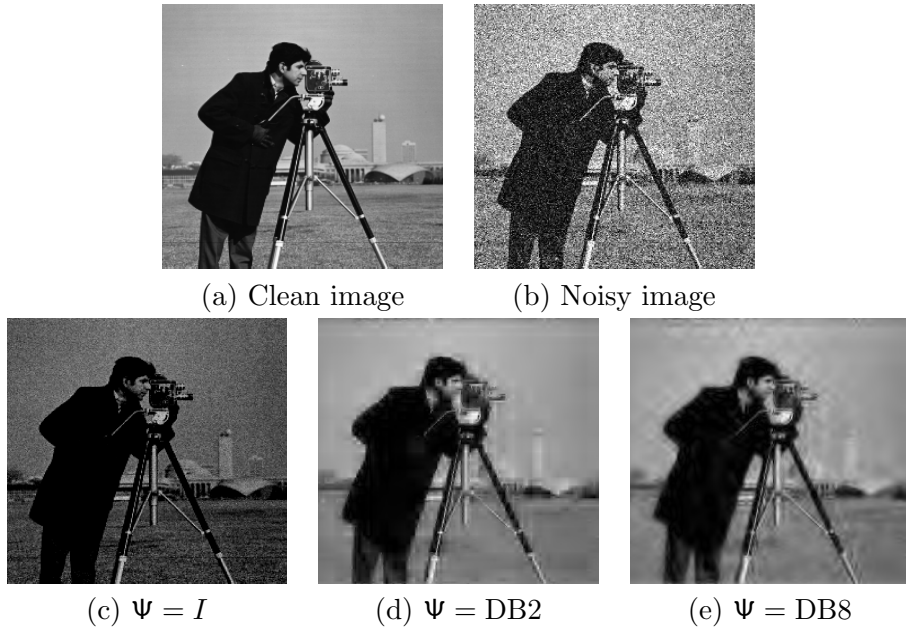


Figure 6.4. Dictionary selection for an image denoising problem solved by proximal nested sampling (test image is cameraman). First row shows the clean image and noisy image. Second row shows the posterior mean images recovered by proximal nested sampling for priors with (sparsifying) transforms $\Psi = I$, $DB2$ and $DB8$, respectively, where the log-prior reads $f(x) = \mu \|\Psi^\dagger x\|_1$. By eye, both $DB2$ and $DB8$ wavelets provide superior reconstruction fidelity compared to $\Psi = I$. The model $\Psi = DB2$ may also be judged to provide slightly superior performance to $\Psi = DB8$.

Table 6.1

Marginal likelihood (Bayesian evidence) values computed by proximal nested sampling for Bayesian model selection of the sparsifying dictionary for an image denoising problem (see Fig. 6.4 for corresponding reconstructed images). Sparsity-promoting (non-differentiable) priors are considered with (sparsifying) transforms $\Psi = I$, $DB2$ and $DB8$. Comparing models, Bayesian model selection afforded by proximal nested sampling suggests the model with the $DB2$ dictionary is superior, followed by $DB8$, both of which are far superior to the case where $\Psi = I$, which agrees with the RMSE (root mean square error) values and assessment performed by eye, which require the ground truth to be known.

Prior	$\log \mathcal{Z}$	RMSE
$\Psi = I$	$-6.54 \times 10^4 \pm 0.08$	41.07
$\Psi = DB2$	$-3.06 \times 10^4 \pm 0.09$	14.29
$\Psi = DB8$	$-3.09 \times 10^4 \pm 0.09$	14.51

Table 6.1 shows that the model with $\Psi = I$ possesses the smallest marginal likelihood value. This implies that for this denoising problem the model with $\Psi = I$ is inferior to models where Ψ is set to $DB2$ and $DB8$. Moreover, the marginal likelihood difference between models where Ψ is set to $DB2$ or $DB8$ is not dramatic, nevertheless this implies that $DB2$ is preferred. These findings inferred by Bayesian model selection agree with the RSME values computed for each model, where the model with $\Phi = DB2$ is slightly preferred over $DB8$, and both

models with DB2 and DB8 are highly preferred over the model with $\Phi = I$ (recall that in practice it is not possible to compute the RMSE since it requires knowledge of the underlying ground truth). Furthermore, the model preferences inferred by proximal nested sampling also agree with the assessment of reconstructed image quality by-eye discussed above. The results obtained are consistent with common knowledge that it is typically more effective to denoise a natural image using a prior that promotes sparsity in some (sparsifying) transform domain (e.g. a wavelet domain) rather than in the image domain itself. The computation time for the problem with $\Psi = I$ is approximately 10 minutes, and for the problem with $\Psi = \text{DB2}$ or DB8 is approximately 60 minutes.

In high-dimensional settings note that Bayes factors can be very large due to the concentration of probability in high-dimensions, hence it is not meaningful to consider traditional scales for assessing model comparisons such as the Jeffery's scale [29]. Instead, we recommend comparing marginal likelihood values directly.

6.3.2. Prior model selection in image reconstruction: regularisation parameter selection. We now apply proximal nested sampling to a standard reconstruction problem and, firstly, consider the selection of the regularisation parameter μ defining the width of the prior. It is typically very challenging to optimally set the regularisation parameter μ , which controls the strength of prior knowledge and plays a key role in reconstruction quality. Consider noisy observations (noisy measurements)

$$(6.2) \quad y = \Phi x + w,$$

where w again denotes Gaussian noise with zero mean and $\sigma = \|x\|_\infty 10^{-\text{SNR}/20}$ (standard deviation), with SNR set to 30, and m and d are respectively the dimension of y and image x . Consider the prior $f(x) = \mu \|\Psi^\dagger x\|_1$, with $\Psi = \text{DB8}$, and likelihood $g(x) = \|y - \Phi x\|_2^2 / 2\sigma^2$. For the reconstruction scenario, Φ represents the sensing (measurement) operator. In particular, we consider a measurement model comprising incomplete Fourier measurements (common in radio interferometric and magnetic resonance imaging) defined by the sensing operator $\Phi = \text{MF}$, constructed from the Fourier transform \mathbf{F} followed by a selection mask \mathbf{M} which is generated randomly through the variable density sampling profile [37]. We consider the scenario where only 30% of Fourier coefficients are measured, i.e. $m = 0.3d$. Note that different forms of the mask \mathbf{M} result in different sensing operators Φ .

Fig. 6.5 presents the posterior means recovered by proximal nested sampling (i.e. the reconstructed images) for models with μ set to 10^6 , 10^7 and 10^8 . It is difficult to assess the effectiveness of different regularisation parameters by eye, but on close inspection it may be noticed that the model with $\mu = 10^6$ is superior to the one with $\mu = 10^7$, which is superior to the one with $\mu = 10^8$. The computation time for each problem is approximately 150 minutes.

Table 6.2 presents the marginal likelihood and RMSE values computed for the models with different regularisation parameters μ . The computed marginal likelihood for the model with $\mu = 10^6$ is larger than the value for the model with $\mu = 10^7$, which is larger than the model with $\mu = 10^8$, suggesting the model with $\mu = 10^6$ is preferred. The computed marginal likelihoods are consistent with the model preferences obtained by comparing the RMSE of each model and by visual inspection. Recall that both RMSE and visual comparisons can only be performed here where the ground truth is available and cannot be used for model comparison in practice.

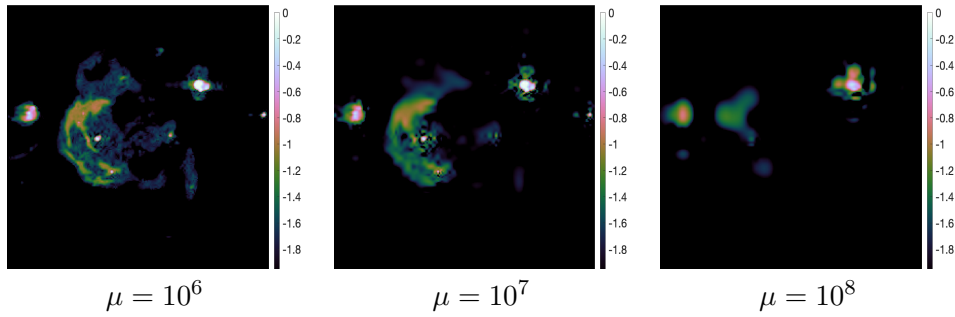


Figure 6.5. Regularisation parameter selection for an image reconstruction problem solved by proximal nested sampling (test image is $W28$ radio galaxy). Images from left to right are the posterior mean images recovered by proximal nested sampling for μ in the prior definition set to 10^6 , 10^7 and 10^8 , respectively. The data y are generated by measuring 30% of noisy Fourier coefficients of the test image. On close inspection it may be noticed that reconstruction for model with $\mu = 10^6$ is superior to the one with $\mu = 10^7$, which is superior to the one with $\mu = 10^8$.

Table 6.2

Marginal likelihood (Bayesian evidence) values computed by proximal nested sampling for Bayesian model selection of the regularisation parameter μ for an image reconstruction problem (see Fig. 6.5 for corresponding reconstructed images). Prior definition with μ set to 10^6 , 10^7 and 10^8 , respectively, are considered. Comparing models, Bayesian model selection afforded by proximal nested sampling suggests the model with $\mu = 10^6$ is superior to the one with $\mu = 10^7$, which is superior to the one with $\mu = 10^8$, which agrees with the RMSE (root mean square error) values and assessment performed by eye, which require the ground truth to be known.

μ	$\log \mathcal{Z}$	RMSE
10^6	$-2.61 \times 10^4 \pm 0.09$	1.82
10^7	$-5.39 \times 10^4 \pm 0.09$	2.81
10^8	$-2.90 \times 10^5 \pm 0.09$	6.70

In summary, this example demonstrates that our proximal nested sampling method is capable of selecting superior regularisation parameters for models stemming from high-dimensional inverse problems.

6.3.3. Measurement model selection in image reconstruction. We now apply proximal nested sampling to the same reconstruction problem considered above (i.e. image reconstruction from noisy and incomplete Fourier measurements) but focus on the problem of misspecification of the measurement model Φ . Noisy observations Y are generated by (6.2), measuring 10% of Fourier coefficients, i.e. with $m = 0.1d$.

We use the ground truth model M_{truth} to simulate observation data y . However, when solving the resulting inverse problem we consider a number of different measurement models, not only the ground truth model M_{truth} but also misspecified models M_γ , where $\gamma > 0$ encodes the level of misspecification.

The method by which the model is misspecified is motivated by radio interferometric imaging. In radio interferometry, the coordinates of the Fourier coefficients acquired by the telescope are measured in units of (radio) wavelength. If the wavelength at which observations are made is misspecified, the coordinates of the Fourier coefficients acquired will be scaled. We

model precisely this type of misspecified model here to represent the case where the instrument wavelength is not calibrated accurately.

An incorrectly specified wavelength then simply acts to modify the mask of the ground truth measurement model M_{truth} . The misspecified model corresponding to mask M_γ , for misspecification parameter γ , is generated by extending every measured position in M_{truth} radially. Specifically, every measured position is extended radially along the line connecting it to the origin to a length of γd_j , $j \in \Omega_{\text{mask}}$, where γ is the misspecification scaling factor, d_j is the distance from the original measured position j to the origin in M_{truth} , and Ω_{mask} is the set which contains all the measured positions. It is worth mentioning that the larger the scaling factor γ , the larger the distortion of M_γ from the ground truth M_{truth} . Note also that $\gamma = 0$ corresponds to a correctly specified model, i.e. $M_{\gamma=0} = M_{\text{truth}}$.

For proximal nested sampling, the number of the live samples N_{live} and dead samples N is respectively set to 2×10^3 and 3×10^4 with thinning factor 10^2 , which is sufficient to ensure convergence. Regularisation parameter $\mu = 10^8$ is used for these experiments.

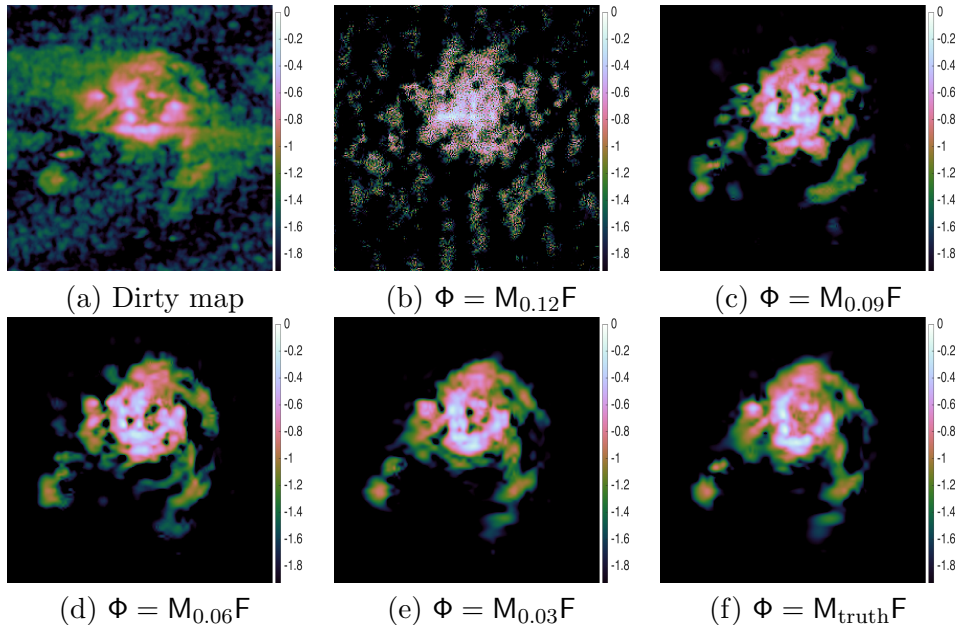


Figure 6.6. Measurement model misspecification for an image reconstruction problem solved by proximal nested sampling (test image is $M31$ radio galaxy). Panel (a): dirty (back-projected) image $\Phi^\dagger Y$; Panels (b)–(f): posterior mean images recovered by proximal nested sampling for misspecified models M_γ , where increasing $\gamma > 0$ corresponds to increasing levels of misspecification (and $\gamma = 0$ corresponds to the ground truth model). It is apparent by eye that the posterior mean image recovered with the ground truth model is the best and that the quality of the recovered posterior mean image degrades as the size of the misspecification scale parameter γ increases.

Fig. 6.6 presents the posterior means recovered (i.e. the reconstruction images) for models with $\Phi_\gamma = M_\gamma F$ and $\Phi = M_{\text{truth}} F$. Here misspecified models $M_{0.12}$, $M_{0.09}$, $M_{0.06}$ and $M_{0.03}$ are generated for misspecification scaling factors γ with values of 0.12, 0.09, 0.06 and 0.03, respectively. It is apparent by eye that the posterior mean image recovered with the ground truth model is the best and that the quality of the recovered posterior mean image degrades

as the size of the misspecification scale parameter γ increases. The computation time for each problem is approximately 150 minutes.

Table 6.3

Marginal likelihood (Bayesian evidence values computed by proximal nested sampling for Bayesian model selection for measurement model misspecification for an image reconstruction problem (see Fig. 6.6 for corresponding reconstructed images). Misspecified models are denoted M_γ , where increasing $\gamma > 0$ corresponds to increasing levels of misspecification (and $\gamma = 0$ corresponds to the ground truth model). Comparing models, Bayesian model selection afforded by proximal nested sampling suggests the model with the lowest misspecification parameter γ is always preferred, which also agrees with the RMSE (root mean square error) values and assessment performed by eye, which require the ground truth to be known.

Likelihood	$\log \mathcal{Z}$	RMSE
$\Phi = M_{\text{truth}} F$	$-4.47 \times 10^3 \pm 0.08$	3.40
$\Phi = M_{0.03} F$	$-4.88 \times 10^3 \pm 0.08$	7.85
$\Phi = M_{0.06} F$	$-5.63 \times 10^3 \pm 0.08$	12.01
$\Phi = M_{0.09} F$	$-9.21 \times 10^3 \pm 0.07$	15.71
$\Phi = M_{0.12} F$	$-1.44 \times 10^4 \pm 0.08$	18.08

Table 6.3 presents the marginal likelihood and RMSE values computed for the different models considered. The computed marginal likelihood is largest when the correct ground truth model is adopted in the likelihood. As the misspecification parameter γ is increased (corresponding to greater misspecification and less accurate models), the corresponding computed marginal likelihood values monotonically decrease (become more negative). For Bayesian model comparison, the model with the lowest misspecification parameter γ is always preferred. The computed marginal likelihoods are consistent with the model preferences obtained by comparing the RMSE of each model and by visual inspection (although recall that such tests cannot be used for model comparison in practice when the ground truth is not known).

7. Conclusions. Nested sampling provides an efficient computational framework to estimate the marginal likelihood (Bayesian evidence) for Bayesian model selection. It effectively re-parameterises the marginal likelihood into a one-dimensional integral of the likelihood with respect to the enclosed prior volume. The challenge of nested sampling is to sample from the prior distribution subject to a hard likelihood constraint. A variety of successful techniques have been developed to perform such sampling in low and moderate dimensional problems. However, existing approaches are not directly useful for imaging applications because they scale poorly to large problems and struggle to support models that are not smooth.

In this article we presented the proximal nested sampling method that is specifically designed for imaging models that are log-concave and potentially very high-dimensional ($d = 10^6$ and beyond), and that can handle models that are not smooth. This is achieved by exploiting tools from proximal calculus and Moreau-Yosida regularisation to efficiently sample from the prior subject to the hard likelihood constraint through a proximal MCMC approach. The resulting Markov chain iterations combine a gradient step that approximates a Langevin SDE that scales efficiently to large problems, with a projection term that acts to push the Markov chain back into the likelihood constraint set if it wanders outside of it, and a Metropolis-Hastings correction step to ensure the hard likelihood constraint is satisfied.

The proposed proximal nested sampling framework was implemented and validated on a Gaussian model for which the marginal likelihood could be calculated in closed-form, showing excellent agreement between values computed analytical and by proximal nested sampling, even in very high dimensions. The use of proximal nested sampling for principled Bayesian model selection was then showcased on a variety of imaging problems with non-smooth sparsity-promoting prior distributions. In particular, model selection problems were considered related to dictionary selection, selection of the regularisation parameter, and selection of the appropriate measurement model when it may be misspecified.

Proximal nested sampling allows Bayesian model selection to be performed at a much higher dimension than that was previously possible, while also supporting non-smooth priors that are widely used in imaging. It is our hope that proximal nested sampling will thus find widespread use for high-dimensional Bayesian model selection, particularly in the imaging sciences.

Acknowledgment. This work was supported by the Leverhulme Trust and by EPSRC (EP/T007346/1).

Appendix I. The volume of the prior $f(x) = \mu\|\Psi^\dagger x\|_2^2$ with $\Psi = I$ is

$$\begin{aligned}
 (7.1) \quad V &= \int_{-\infty}^{\infty} \exp(-\mu\|x\|_2^2) dx \\
 &= \int_{-\infty}^{\infty} \exp\left(-\frac{1}{2}2\mu x^\top x\right) dx \\
 &= \sqrt{\frac{(2\pi)^d}{(2\mu)^d}}.
 \end{aligned}$$

For the prior $f(x) = \mu\|\Psi^\dagger x\|_2^2$ with $\Psi = I$ and the likelihood $g(x) = \|y - \Phi x\|_2^2/2\sigma^2$ with $\Phi = I$, the Bayesian evidence value has the following closed-form representation:

$$\begin{aligned}
 (7.2) \quad &\frac{1}{V} \int_{-\infty}^{\infty} \exp(-\mu\|x\|_2^2) \exp(-\|y - x\|_2^2/2\sigma^2) dx \\
 &= \frac{1}{V} \int_{-\infty}^{\infty} \exp\left(-\mu\|x\|_2^2 - \|y - x\|_2^2/2\sigma^2\right) dx \\
 &= \frac{1}{V} \int_{-\infty}^{\infty} \exp\left(-(\mu + 1/2\sigma^2)x^\top x + y^\top x/\sigma^2 - y^\top y/2\sigma^2\right) dx \\
 &= \frac{1}{V} \exp\left(-\frac{y^\top y}{2\sigma^2}\right) \int_{-\infty}^{\infty} \exp\left(-\frac{1}{2}(2\mu + 1/\sigma^2)x^\top x + y^\top x/\sigma^2\right) dx \\
 &= \frac{1}{V} \sqrt{\frac{(2\pi)^d}{(2\mu + 1/\sigma^2)^d}} \exp\left(-\frac{y^\top y}{2\sigma^2}\right) \exp\left(\frac{1}{2} \frac{1}{2\mu + 1/\sigma^2} \frac{y^\top y}{\sigma^4}\right),
 \end{aligned}$$

whose logarithmic value is

$$(7.3) \quad \log \sqrt{\frac{(2\pi)^d}{(2\mu + 1/\sigma^2)^d}} + \left(-\frac{y^\top y}{2\sigma^2}\right) + \left(\frac{1}{2} \frac{1}{2\mu + 1/\sigma^2} \frac{y^\top y}{\sigma^4}\right) - \log V.$$

REFERENCES

- [1] B. J. BREWER, L. B. PÁRTAY, AND G. CSÁNYI, *Diffusive nested sampling*, Statistics and Computing, 21 (2011), pp. 649–656.
- [2] N. BROSSE, A. DURMUS, ÉRIC MOULINES, AND M. PEREYRA, *Sampling from a log-concave distribution with compact support with proximal langevin monte carlo*, in Proceedings of the 2017 Conference on Learning Theory, S. Kale and O. Shamir, eds., vol. 65 of Proceedings of Machine Learning Research, Amsterdam, Netherlands, 07–10 Jul 2017, PMLR, pp. 319–342, <http://proceedings.mlr.press/v65/brosse17a.html>.
- [3] X. CAI, R. CHAN, AND T. ZENG, *A Two-Stage Image Segmentation Method Using a Convex Variant of the Mumford-Shah Model and Thresholding*, SIAM Journal on Imaging Sciences, 6 (2013), pp. 368–390.
- [4] X. CAI, M. PEREYRA, AND J. D. MCEWEN, *Uncertainty quantification for radio interferometric imaging I: proximal-MCMC methods*, Monthly Notices of the Royal Astronomical Society (MNRAS), 480 (2018), pp. 4154–4169.
- [5] X. CAI, M. PEREYRA, AND J. D. MCEWEN, *Uncertainty quantification for radio interferometric imaging II: MAP estimation*, Monthly Notices of the Royal Astronomical Society (MNRAS), 480 (2018), pp. 4170–4182.
- [6] X. CAI, L. PRATLEY, AND J. D. MCEWEN, *Online radio interferometric imaging: assimilating and discarding visibilities on arrival*, Monthly Notices of the Royal Astronomical Society (MNRAS), 485 (2019), pp. 4559–4572.
- [7] A. CHAMBOLLE AND T. POCK, *An introduction to continuous optimization for imaging*, Acta Numerica, 25 (2016), pp. 161–319, <https://doi.org/10.1017/s096249291600009x>, <https://doi.org/10.1017/s096249291600009x>.
- [8] S. CHIB, *Marginal likelihood from the Gibbs output*, Journal of the American Statistical Association, 90 (1995), pp. 1313–1321.
- [9] S. CHIB AND I. JELIAZKOV, *Marginal likelihood from the Metropolis-Hastings output*, Journal of the American Statistical Association, 96 (2001), pp. 270–281.
- [10] M. A. CLYDE, J. O. BERGER, F. BULLARD, E. B. FORD, W. H. JEFFERYS, AND R. LUO, *Current challenges in Bayesian model choice*, Statistical Challenges in Modern Astronomy IV ASP Conference Series, 371 (2007), pp. 224–240.
- [11] P. L. COMBETTES AND J. C. PESQUET, *Proximal Splitting Methods in Signal Processing*, ArXiv e-prints, (2010), <https://arxiv.org/abs/0912.3522v4>.
- [12] A. DURMUS, E. MOULINES, AND M. PEREYRA, *Efficient Bayesian computation by proximal Markov chain Monte Carlo: when Langevin meets Moreau*, SIAM Journal Imaging Sciences, 1 (2018), pp. 473–506.
- [13] F. FEROZ AND M. P. HOBSON, *Multimodal nested sampling: an efficient and robust alternative to MCMC methods for astronomical data analysis*, Monthly Notices of the Royal Astronomical Society (MNRAS), 384 (2008), pp. 449–463.
- [14] F. FEROZ, M. P. HOBSON, AND M. BRIDGES, *MULTINEST: an efficient and robust Bayesian inference tool for cosmology and particle physics*, Monthly Notices of the Royal Astronomical Society (MNRAS), 398 (2009), pp. 1601–1614.
- [15] F. FEROZ AND J. SKILLING, *Exploring multi-modal distributions with nested sampling*, AIP Conference Proceedings, 1553 (2013), pp. 106–113.
- [16] N. FRIEL AND J. WYSE, *Estimating the evidence – a review*, Statistica Neerlandica, (2012), <https://doi.org/DOI:10.1111/j.1467-9574.2011.00515.x>.
- [17] P. J. GREEN, *Reversible jump markov chain monte carlo computation and bayesian model determinatio*, Biometrika, 82 (1995), pp. 711–732.
- [18] P. J. GREEN, K. LATUŚZYNSKI, M. PEREYRA, AND C. P. ROBERT, *Bayesian computation: a summary of the current state, and samples backwards and forwards*, Statistics and Computing, 25 (2015), pp. 835–862.
- [19] W. J. HANDLEY, M. P. HOBSON, AND A. N. LASENBY, *POLYCHORD: nested sampling for cosmology*, Monthly Notices of the Royal Astronomical Society: Letters, 450 (2015), p. L61–L65.
- [20] B. HARROUE, *Approche bayésienne pour la sélection de modèles : application à la restauration d'image*, PhD thesis, 2020, <http://www.theses.fr/2020BORD0127>. Thèse de doctorat dirigée par Giovannelli, Jean-François et Pereyra, Marcelo Automatique, Productique, Signal et Image, Ingénierie cognitive

Bordeaux 2020.

[21] J. KAPIO AND E. SOMERSALO, *Statistical and Computational Inverse Problems*, Springer, New-York, (2005).

[22] K. KAMARY, K. MENGERSEN, C. P. ROBERT, AND J. ROUSSEAU, *Testing hypotheses via a mixture estimation model*, 2018, <https://arxiv.org/abs/1412.2044>.

[23] S. LUNZ, A. HAUPTMANN, T. TARVAINEN, C.-B. SCHÖNLIEB, AND S. ARRIDGE, *On Learned Operator Correction in Inverse Problems*, SIAM Journal Imaging Sciences, 14 (2021), pp. 92–127.

[24] J. D. MCEWEN, C. G. R. WALLIS, AND PRICE, M. A., *Machine learning assisted marginal likelihood estimation: the learnt harmonic mean estimator*, in prep., (2020).

[25] P. MUKHERJEE, D. PARKINSON, AND A. R. LIDDLE, *A nested sampling algorithm for cosmological model selection*, The Astrophysical Journal, 638 (2006), pp. L51–L54.

[26] R. NEAL, *Annealed importance sampling*, Statistics and Computing, 11 (2001), pp. 125–139.

[27] R. NEAL, *Slice sampling*, Annals of Statistics, 31 (2003), pp. 705–767.

[28] R. NEAL, *MCMC using Hamiltonian dynamics*, ArXiv e-prints, (2012), <https://arxiv.org/abs/1206.1901>.

[29] S. NESSERIS AND J. GARCÍA-BELLIDO, *Is the Jeffreys' scale a reliable tool for Bayesian model comparison in cosmology?*, Journal of Cosmology and Astroparticle Physics, 2013 (2013), pp. 036–036.

[30] M. A. NEWTON AND A. E. RAFTERY, *Approximate Bayesian inference with the weighted likelihood bootstrap*, Journal of the Royal Statistical Society, 56 (1994), pp. 3–48.

[31] J. O'RUANAIDH AND W. J. FITZGERALD, *Numerical Bayesian methods applied to signal processing*, Springer-Verlag New York, 1996.

[32] N. PARIKH AND S. BOYD, *Proximal algorithms*, Foundations and Trends in Optimization, 1 (2013), pp. 123–231.

[33] M. PEREYRA, *Proximal Markov chain Monte Carlo algorithms*, Statistics and Computing, 26 (2016), pp. 745–760.

[34] M. PEREYRA, *Maximum-a-Posteriori estimation with bayesian confidence regions*, SIAM Journal Imaging Sciences, 10 (2017), pp. 285–302.

[35] M. PEREYRA AND S. MC LAUGHLIN, *Comparing bayesian models in the absence of ground truth*, in 2016 24th European Signal Processing Conference (EUSIPCO), 2016, pp. 528–532, <https://doi.org/10.1109/EUSIPCO.2016.7760304>.

[36] M. PEREYRA, P. SCHNITER, E. CHOUZENOUX, J.-C. PESQUET, J.-Y. TOURNERET, A. O. HERO, AND S. MC LAUGHLIN, *A survey of stochastic simulation and optimization methods in signal processing*, IEEE Journal of Selected Topics in Signal Processing, 10 (2016), pp. 224–241, <https://doi.org/10.1109/JSTSP.2015.2496908>.

[37] G. PUY, P. VANDERGHEYNST, AND Y. WIAUX, *On Variable Density Compressive Sampling*, IEEE Signal Processing Letters, 18 (2011), pp. 595–598.

[38] C. P. ROBERT, *The Bayesian Choice*, Springer-Verlag New York, 2007.

[39] C. P. ROBERT AND G. CASELLA, *Monte Carlo Statistical Methods*, Springer-Verlag New York, 2004.

[40] L. RUDIN, S. OSHER, AND E. FATEMI, *Nonlinear total variation based noise removal algorithms*, Physica D, 60 (1992), pp. 259–268.

[41] D. SIVIA AND J. SKILLING, *Data Analysis: A Bayesian Tutorial*, Oxford Science Publications, (2006).

[42] J. SKILLING, *Nested sampling for general Bayesian computation*, Bayesian Analysis, 1 (2006), pp. 833–859.

[43] L. TIERNEY AND J. B. KADANE, *Accurate approximations for posterior moments and marginal densities*, Journal of the American Statistical Association, 81 (1986), pp. 82–86.

[44] R. TROTTA, *Applications of Bayesian model selection to cosmological parameters*, Monthly Notices of the Royal Astronomical Society (MNRAS), 378 (2007), pp. 72–82.

[45] L. VARGAS, M. PEREYRA, AND K. C. ZY GALAKIS, *Accelerating proximal markov chain monte carlo by using an explicit stabilised method*, 2020. to appear.

[46] A. F. VIDAL, V. D. BORTOLI, M. PEREYRA, AND A. DURMUS, *Maximum likelihood estimation of regularization parameters in high-dimensional inverse problems: An empirical bayesian approach part i: Methodology and experiments*, SIAM Journal on Imaging Sciences, 13 (2020), pp. 1945–1989, <https://doi.org/10.1137/20m1339829>, <https://doi.org/10.1137/20m1339829>.

[47] Q. ZHOU, T. YU, X. ZHANG, AND J. LI, *Bayesian Inference and Uncertainty Quantification for Medical Image Reconstruction with Poisson Data*, SIAM Journal Imaging Sciences, 13 (2020), pp. 29–52.